

NIST Measurement Services:

Calibration Service of Optoelectronic Frequency Response at 1319 nm for Combined Photodiode/RF Power Sensor Transfer Standards

**NIST
Special
Publication
250-51**

Paul D. Hale and C. M. Wang

U.S. Department of Commerce
Technology Administration
National Institute of Standards and Technology

The National Institute of Standards and Technology was established in 1988 by Congress to “assist industry in the development of technology . . . needed to improve product quality, to modernize manufacturing processes, to ensure product reliability . . . and to facilitate rapid commercialization . . . of products based on new scientific discoveries.”

NIST, originally founded as the National Bureau of Standards in 1901, works to strengthen U.S. industry’s competitiveness; advance science and engineering; and improve public health, safety, and the environment. One of the agency’s basic functions is to develop, maintain, and retain custody of the national standards of measurement, and provide the means and methods for comparing standards used in science, engineering, manufacturing, commerce, industry, and education with the standards adopted or recognized by the Federal Government.

As an agency of the U.S. Commerce Department’s Technology Administration, NIST conducts basic and applied research in the physical sciences and engineering, and develops measurement techniques, test methods, standards, and related services. The Institute does generic and precompetitive work on new and advanced technologies. NIST’s research facilities are located at Gaithersburg, MD 20899, and at Boulder, CO 80303. Major technical operating units and their principal activities are listed below. For more information contact the Publications and Program Inquiries Desk, 301-975-3058.

Office of the Director

- National Quality Program
- International and Academic Affairs

Technology Services

- Standards Services
- Technology Partnerships
- Measurement Services
- Technology Innovation
- Information Services

Advanced Technology Program

- Economic Assessment
- Information Technology and Applications
- Chemical and Biomedical Technology
- Materials and Manufacturing Technology
- Electronics and Photonics Technology

Manufacturing Extension Partnership Program

- Regional Programs
- National Programs
- Program Development

Electronics and Electrical Engineering Laboratory

- Microelectronics
- Law Enforcement Standards
- Electricity
- Semiconductor Electronics
- Electromagnetic Fields¹
- Electromagnetic Technology¹
- Optoelectronics¹

Chemical Science and Technology Laboratory

- Biotechnology
- Physical and Chemical Properties²
- Analytical Chemistry
- Process Measurements
- Surface and Microanalysis Science

Physics Laboratory

- Electron and Optical Physics
- Atomic Physics
- Optical Technology
- Ionizing Radiation
- Time and Frequency¹
- Quantum Physics¹

Materials Science and Engineering Laboratory

- Intelligent Processing of Materials
- Ceramics
- Materials Reliability¹
- Polymers
- Metallurgy
- NIST Center for Neutron Research

Manufacturing Engineering Laboratory

- Precision Engineering
- Automated Production Technology
- Intelligent Systems
- Fabrication Technology
- Manufacturing Systems Integration

Building and Fire Research Laboratory

- Structures
- Building Materials
- Building Environment
- Fire Safety Engineering
- Fire Science

Information Technology Laboratory

- Mathematical and Computational Sciences²
- Advanced Network Technologies
- Computer Security
- Information Access and User Interfaces
- High Performance Systems and Services
- Distributed Computing and Information Services
- Software Diagnostics and Conformance Testing
- Statistical Engineering

¹At Boulder, CO 80303.

²Some elements at Boulder, CO.

NIST Special Publication 250-51

NIST MEASUREMENT SERVICES:

Calibration Service of Optoelectronic Frequency Response at 1319 nm for Combined Photodiode/RF Power Sensor Transfer Standards

Paul D. Hale and C. M. Wang

Optoelectronics Division
Electronics and Electrical Engineering Laboratory
National Institute of Standards and Technology
325 Broadway
Boulder, CO 80303-3328

December 1999



U.S. Department of Commerce
William M. Daley, Secretary

Technology Administration
Dr. Cheryl L. Shavers, Under Secretary of Commerce for Technology

National Institute of Standards and Technology
Raymond G. Kammer, Director

National Institute of Standards and Technology Special Publication 250-51
Natl. Inst. Stand. Technol. Spec. Publ. 250-51, 51 pages (Dec. 1999)
CODEN: NSPUE2

U.S. GOVERNMENT PRINTING OFFICE
WASHINGTON: 1999

For sale by the Superintendent of Documents, U.S. Government Printing Office, Washington, DC 20402-9325

Contents

1. Introduction	1
2. Principle of heterodyne frequency response measurements	2
2.1 Photodiode with access to bias monitor	3
2.2 Combined photodiode/rf power sensor transfer standard	5
3. Nd:YAG heterodyne measurement system	6
3.1 Basic setup and swept operation	6
3.2 Phase-locked operation	11
3.3 Power matching	12
4. Uncertainty in combined photodiode/power sensor normalized response	13
4.1 Type A uncertainties	13
Repeatability	13
Offset correction	17
Environmental conditions	19
4.2 Type B uncertainties	24
Meter range scaling	24
Meter offset	24
Optical power drift (power matching)	24
Bias current measurement	24
Power sensor noise	24
Reference power uncertainty	25
Gunn oscillator frequency drift	25
Hysteresis	25
Relative intensity noise	25
5. Quality Control	26
5.1 Calibration notebook	26
5.2 Checks on each calibration	26
5.3 Periodic checks	26
Power stability	26
Gunn oscillator frequency	26
Check standards	26
5.4 Future system changes	27
5.5 Transfer standards which are suitable for calibration	27
6. References	27

Appendix A: Use of transfer standard in a ratio system	30
A.1 Application of heterodyne formalism to arbitrary modulation depth	30
A.2 Calibration transfer using ratio measurements	31
A.3 Sources of uncertainty in ratio measurement system	33
Type of photoreceiver specimen	33
Spurious harmonics	33
Relative intensity noise	33
Wavelength dependence	33
Reference	33
Appendix B: Heterodyne system with unequal powers	35
Appendix C: The meaning of normalized response and 0 dB	36
Appendix D: Photoreceiver with no access to bias monitor	37
D.1 Expression of absolute responsivity in terms of measured quantities	37
D.2 Uncertainties of amplified receiver/power sensor combined response	37
Coupling ratio	38
Receiver linearity	38
Receiver stability	38
Receiver noise	38
Appendix E. Sample calibration certificate	40
Appendix F. Shipping instructions	47

Calibration Service of Optoelectronic Frequency Response at 1319 nm for Combined Photodiode/rf Power Sensor Transfer Standards

Paul D. Hale and C. M. Wang

National Institute of Standards and Technology
Boulder, Colorado 80303

This document describes the Calibration Service provided by the National Institute of Standards and Technology (NIST) for optoelectronic frequency response transfer standards and their use in measuring optical modulation depth. The service supports the calibration of transfer standards consisting of a pigtailed photodiode, with access to the bias current, combined with an rf power sensor over the frequency range of 300 kHz to 55 GHz at 1319 nm. Typical measurement uncertainties are about 0.05 dB, which includes measurement repeatability, rf power meter scaling accuracy and offset, optical power drift, bias current measurement, and power sensor noise. The measurement technique, based on the heterodyne beat note between two single-frequency Nd:YAG lasers operating at 1319 nm, is reviewed and its implementation is described. A detailed analysis of sources of error and estimates of uncertainty are presented. Use of the transfer standard for measuring an arbitrary optical modulation depth is described along with some design considerations to achieve the lowest possible transfer uncertainty. A modification of the calibration service that allows calibration of photoreceivers that do not provide access to the bias current is also described. This modification, offered as a Special Test, allows the absolute responsivity of the photoreceiver to be measured, but with degraded uncertainty due to repeatability of the optical insertion loss of the fiber connectors.

Key words: calibration; frequency response; modulation depth; optical receiver; photodiode; reference receiver; transfer standard

1. Introduction

Increased commercial availability of optoelectronic devices and test equipment requires the availability of accurate and inexpensive optoelectronic frequency response calibrations that are traceable to national standards. Examples of this need are the standard test receivers used for SDH/SONET (synchronous digital hierarchy/synchronous optical network), Fibre Channel, and Gigabit Ethernet that are specified [1] as having a fourth-order Bessel-Thompson filter response with tolerances [2], [3] as low as ± 0.3 dB to ± 0.5 dB. Instrumentation for analog applications such as CATV have comparable tolerances. Our customers prefer transfer standard receivers that are calibrated with uncertainties that are at least a factor of 4 smaller. Until recently, uncertainties this low were not possible [4], [5].

In the past, photoreceiver frequency response measurements have had high uncertainties for two reasons: inaccurate knowledge of the optical stimulus and large uncertainties in the microwave power measurement. With careful attention to system performance, uncertainties around 0.12 dB to 0.45 dB can be achieved [5]. This accuracy is not adequate to support the ± 0.3 dB SDH/SONET tolerance specifications with adequate confidence.

In a well designed heterodyne measurement system, the variation in optical stimulus can be reduced to ± 0.0023 dB (coverage factor $k = 1$). Typical rf power sensor calibration uncertainties are about a factor of 15 or 20 higher (for $k = 1$). Uncertainties due to mismatch can be 0.1 dB or higher. Mismatch errors can be corrected, but it is unclear whether the uncertainty in the corrections is low enough to give adequately improved uncertainty. If the uncertainty due to rf calibration and impedance mismatch could be eliminated, the overall optoelectronic response uncertainty could be significantly reduced.

In this work, we describe a method for calibrating a photoreceiver frequency response transfer standard with the low inherent uncertainty of a Nd:YAG heterodyne system. This is achieved by combining a photoreceiver with a microwave power sensor and calibrating the response of the combined unit, eliminating rf sensor calibration and mismatch uncertainties. The measured response is normalized to the dc electrical power generated in the photodiode to give the lowest possible uncertainty. The Nd:YAG heterodyne measurement system is also described along with a detailed uncertainty analysis for calibration of a combined photoreceiver/power sensor transfer standard. The theory for measuring an unknown device against the transfer standard and measurement of modulation depth is also derived.

Calibration of frequency response normalized to the optical power is also described. This type of normalization gives absolute responsivity, but with a degraded uncertainty, and is especially suited to calibrations of amplified photoreceivers. It is offered as a Special Test because the uncertainties due to fiber connector insertion loss can not be fully evaluated.

2. Principle of heterodyne frequency response measurements

The advantages and disadvantages of various methods for characterizing photoreceivers have been discussed by several authors [4], [6], [7]. The main advantages of the heterodyne method are that the optical modulation is completely calculable from fundamental principles, it gives results directly in the frequency domain where many industrial specifications are written, and tuning ranges are available over 65 GHz or more. The heterodyne principle is based on a property of all optical quantum detectors: the current generated by the detector is proportional to the time-averaged energy flow $\langle S \rangle$ integrated over the surface of the detector. Here S is the Poynting vector and its time average (assuming a monochromatic plane wave) is [8]

$$\langle S \rangle = \frac{1}{2} \sqrt{\frac{\epsilon_0}{\mu_0}} (E \cdot E^*) \hat{k} \quad (1)$$

where ϵ_0 is the permittivity of free space, μ_0 is the permeability of free space, E is the electric field vector, E^* is its complex conjugate, and \hat{k} is a unit vector in the direction of propagation. The heterodyne beat note at frequency f is generated by mixing signals from two “single-frequency” lasers as shown in figure 1. If the laser beams have the same polarization and the curvature and direction of propagation of the laser beams after passing through the beamsplitter are the same (the beams are mode-matched) the electric field incident on the detector can be written as

$$E(x, y, t) = (E_{O1}e^{i\omega t} + E_{O2}e^{i(\omega+2\pi f)t})F_s(x, y) . \quad (2)$$

Equation (2) can then be integrated over the surface of the detector eliminating the spatial dependence in $F_s(x, y)$ to give the power incident on the detector. Let the power delivered to the detector by the i th laser be $P_{O_i} = \frac{1}{2}|E_{O_i}|^2 A (\epsilon_0/\mu_0)^{1/2}$ where $A = \iint |F_s(x, y)|^2 dx dy$ integrated over the area of the detector, and E_{O_i} is the electric field. Then the total power incident on the detector is

$$P_{total}(t) = (P_{O1} + P_{O2}) + 2\sqrt{P_{O1}P_{O2}} \cos(2\pi ft) . \quad (3)$$

Here we have assumed that the power from each laser is constant and that each laser is truly single frequency. The phase relationship between the lasers has also been neglected.

2.1 Photodiode with access to bias monitor

The photodiode in figure 1 is connected to an external bias network and dc blocking capacitor. A dc return path must be provided for the photodiode, either through a bias T or through a resistor or attenuator. The photocurrent generated by the photodiode due to the optical power incident on it is given by

$$\begin{aligned} i_p(f, t) &= (P_{O1} + P_{O2}) R(0) \\ &+ 2\sqrt{P_{O1}P_{O2}} R(f) \cos(2\pi ft + \phi(f)) \\ &= i_{dc} + i_{rf} , \end{aligned} \quad (4)$$

where $R(f)$ is the responsivity of the detector (in A/W) at frequency f and $\phi(f)$ accounts for phase delay in the photodiode, transmission line, and connectors. For the purposes of this

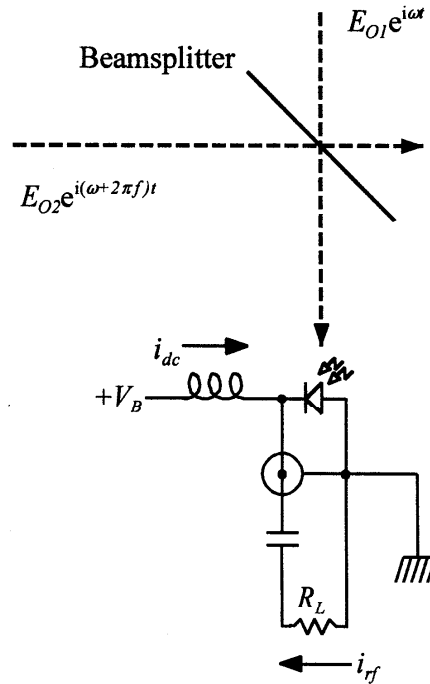


Figure 1. Simple photodiode circuit showing generation of photocurrents.

work phase can be neglected. Equation (4) assumes that the detector is reverse-biased and uses the convention of positive current flowing in the reverse direction of the diode. The first term on the right side is the dc photocurrent, which flows through the bias supply, and the second term is the rf photocurrent, which flows through the rf load (the microwave power sensor) through a dc blocking capacitor. The mean squared photocurrent generated by the photodiode is

$$\begin{aligned}\langle i_p^2(f) \rangle &= (P_{O1} + P_{O2})^2 R^2(0) + 2P_{O1} P_{O2} R^2(f) \\ &= \langle i_{dc}^2 \rangle + \langle i_{rf}^2 \rangle.\end{aligned}\quad (5)$$

If P_{O1} is nearly equal to P_{O2} , then $2(P_{O1}P_{O2})$ is, to first order, equal to $0.5(P_{O1} + P_{O2})^2$, as discussed in Appendix B. The normalized frequency response $\mathfrak{R}^2(f)$ which is defined as $R^2(f)/R^2(0)$, can then be found by taking the ratio of the rf electrical power P_{rf} to half the dc electrical power delivered to a load R_L ,

$$\begin{aligned}\frac{2P_{rf}}{\langle i_{dc}^2 \rangle R_L} &= \frac{\langle i_{rf}^2 \rangle R_L}{0.5 \langle i_{dc}^2 \rangle R_L} \\ &= \frac{2(P_{O1}P_{O2})R^2(f)R_L}{0.5(P_{O1} + P_{O2})^2 R^2(0)R_L} \\ &\approx \frac{R^2(f)}{R^2(0)}.\end{aligned}\quad (6)$$

P_{rf} is a function of frequency. It includes corrections for the sensor calibration factor and electrical mismatch, and is the power that would be delivered to an ideal load R_L [9]. Measurements are typically made with transmission lines and loads with characteristic impedance of 50 Ω ; however these equations also apply to measurements with 75 Ω systems. The normalized frequency response may be quoted in decibels as $20\log[\mathfrak{R}(f)]$. All NIST calibrations report the normalized response in $20\log[\mathfrak{R}(f)]$ format. The electrical bandwidth of the device is where $20\log[\mathfrak{R}(f)]$ falls by 3 dB from the low frequency level [3].

In an ideal measurement $\langle i_{dc}^2 \rangle$ is constant, but in any real measurement system it may vary because of changing optical power coupled to the photodiode. The ratio in eq (6) is insensitive to optical power variations. Using the normalized response also simplifies the measurement apparatus because only the total photocurrent in the photodiode need be monitored instead of the power coupled to the detector from each laser.

The normalized frequency response is an unbiased method for comparing measurements made with different systems. A common practice when comparing frequency response measurements is to add an offset to each curve to make the responses equal at some frequency or over some

range of frequencies. This practice assumes that both systems impart negligible error at that frequency and can be misleading.

Another method of comparison uses the absolute response. This method suffers from connector insertion loss reproducibility and optical power uncertainty. The absolute rf responsivity is calculated from the normalized frequency response by multiplying by the square of the dc responsivity, which is measured separately. Because most fast commercial photodetector packages are pigtailed and connectorized, the uncertainty of the absolute responsivity includes the uncertainty of the fiber connector insertion loss. Variations in fiber connector insertion loss may be high and can contribute to significant uncertainties in the absolute responsivity [10], [11]. A correction must be made for these variations to attain the desired uncertainty. This problem will be discussed further in Appendix D and Chapter 4. High speed detectors that are thin may also have significant wavelength dependence of the absolute responsivity due to interference in the photodiode.

2.2 Combined photodiode/rf power sensor transfer standard

Measurement of a photodiode's unknown frequency response using a photodiode (transfer standard) calibrated using eq (6) includes calibration uncertainty of both the power sensors used to measure P_{rr} from the photodiode transfer standard at NIST and at the customer's laboratory, and calibration uncertainty of the sensor used to measure the photodiode, giving a total expanded uncertainty of 0.2 dB or more for the modulation transfer function. Combined with other factory uncertainties, this may give an unacceptable uncertainty for the intended test system.

The transfer uncertainty can be reduced by calibrating the frequency response of the photodiode combined with the rf power sensor and bias T or attenuator used for dc return. This method totally eliminates uncertainties due to power sensor calibration and impedance mismatch. The combined frequency response $\mathbb{R}^2(f)$ measured on the NIST heterodyne measurement system includes the power sensor calibration factor and impedance mismatch, and is given by

$$\begin{aligned} \mathbb{R}^2(f) &= \frac{\mathfrak{R}^2(f)}{C} \\ &= \frac{P_m}{0.5 \langle i_{dc}^2 \rangle R_L} \end{aligned} \quad (7)$$

In eq (7), P_m is the indication of the power meter after zeroing and calibration against the 50 MHz reference signal (from the power meter) using a calibration factor of 100 %. C is given by

$$C = \frac{1}{k} |1 - \Gamma_{pd} \Gamma_{sensor}|^2, \quad (8)$$

where k is the sensor calibration factor and Γ_{pd} and Γ_{sensor} are complex reflection coefficients. However, C does not need to be known and the power meter reading does not need to be corrected with a frequency dependent calibration factor. The form of C is stated here only for completeness.

The photodiode, attenuator or bias T, and rf power sensor can be left free to be disconnected at the plane of the power sensor connector, or they can be permanently joined. Each of these methods has potential trade-offs. If the power sensor is free to be disconnected, the internal gain of the power meter can be scaled according to the 50 MHz reference source on the power meter. This may be an advantage if the transfer standard will be used to measure modulation depth (see Appendix A). However this introduces uncertainty due to the disconnect/reconnect procedure and can be operator dependent. This uncertainty is a function of frequency.

If the power sensor is kept attached to the photodiode, the internal gain cannot be scaled to the 50 MHz reference source, and long-term drifts in the gain can lead to offsets (on a logarithmic scale) in the response. These offsets can be assumed to be independent of frequency since the measurement is made over a short time relative to the drift. Then the offsets can be corrected using a least-median deviation, as described in Chapter 4. This type of transfer standard calibration would be preferred for measurements that are more concerned with the frequency response at one frequency relative to another frequency than with the “absolute” normalized frequency response. For example, this type of transfer standard could not be used to measure the actual fractional modulation depth of a source, only changes in the modulation depth with frequency (see Appendix A). The choice between these methods is left to the customer.

3. Nd:YAG heterodyne measurement system

3.1 Basic setup and swept operation

The Nd:YAG heterodyne system uses two commercially available single-mode monolithic-ring Nd:YAG lasers operating at 1.319 μm . The system of lasers, mirrors, attenuators, acousto-optic modulator (AOM), and beamsplitters is shown in figure 2. The laser YAG3 is a new high-power model that replaced the laser previously called YAG1. The beam from YAG2 travels through the AOM and is combined with the beam from YAG3 in beamsplitter BS1. The combined beams then go through polarizing isolators. These reduce the effects of optical feedback on the lasers and ensure that the polarization of each laser is the same before entering standard single-mode fiber through variable focus collimators. The collimators have return loss greater than 30 dB to reduce multiple path interference in the fibers. The AOM uses a traveling acoustic wave to diffract a small fraction of the beam from YAG2. This beam is Doppler-shifted down in frequency by 70 MHz and is combined with a small portion of the beam from YAG3 in

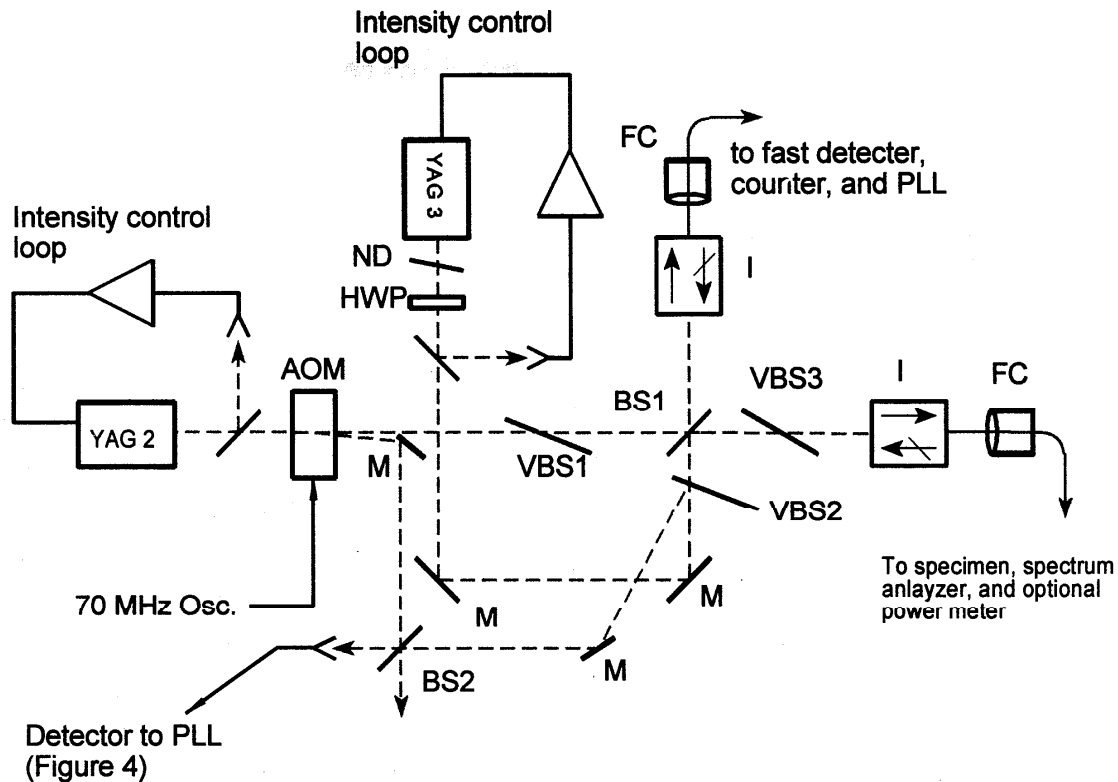


Figure 2. Schematic of heterodyne measurement system. Labeled components are beamsplitter (BS), variable beamsplitter or variable attenuator (VBS), mirror (M), acousto-optic frequency shifter (AOM), neutral density filter (ND), half-wave plate (HWP), isolator (I), and fiber-collimator (FC).

beamsplitter BS2. The resulting beat note, which differs in frequency by 70 MHz from the main signal at BS1, may be used for phase locking the lasers and controlling their frequency difference with a frequency-synthesized signal generator. This option will be discussed in section 3.2.

The frequency of each laser can be tuned thermally to give beat frequencies from nearly dc to greater than 55 GHz; the beats have a short-term bandwidth of less than 3 kHz. The beat frequency is measured with a microwave counter (see figure 3). As the frequency is swept, data are acquired automatically. The data spacing is usually selected to be one-tenth to one-fifth of the customer's requested data spacing. The frequency resolution of the system is limited by the sweep rate, the frequency jitter, and the time constants of the data acquisition equipment. At

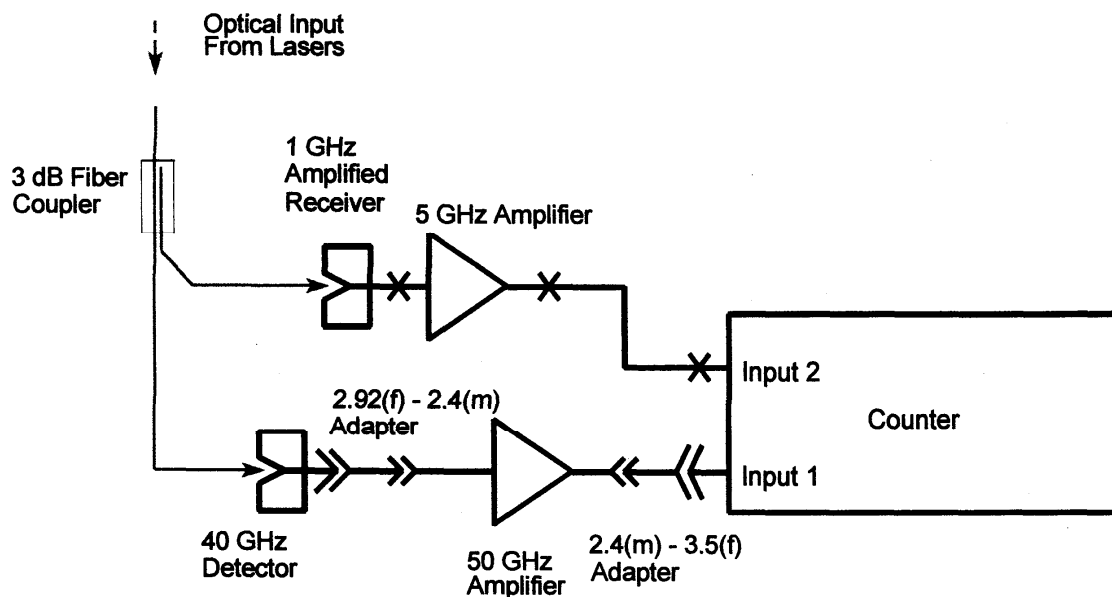


Figure 3. Frequency counter subassembly for operation below 40 GHz. Although input 1 is specified between 500 MHz and 40 GHz, it does operate, with some cut-outs, below 500 MHz. Input 2 operates between 10 Hz and 80 MHz in high Z (1 M Ω) mode and between 10 MHz and 525 MHz in 50 Ω mode. The 3 dB coupler can be omitted and the optical input can go directly into the high bandwidth detector for high bandwidth scans where the detector sensitivity is degraded.

present, the highest resolution achievable in swept mode is about 300 kHz, although the resolution may be considerably worse when the frequency is swept quickly (for example when a much larger data spacing is desired). Higher resolution can be achieved using the phase-locked loop described later in this chapter. Since the frequency range of the rf counter is limited to about 40 GHz, an external mixer is required to down-convert frequencies above 40 GHz to a range where the counter operates. The circuit for down-conversion of frequencies in the 40 to 55 GHz range is shown in figure 4. The beat signal is generated in a 40 GHz bandwidth detector and amplified in a 50 GHz bandwidth amplifier. This signal then enters the rf port of the mixer. The LO (local oscillator) is provided by a Gunn oscillator operating at about 62.15 GHz. The down-converted signal from the IF port is then amplified with a 26 GHz bandwidth amplifier and fed into channel 1 of the rf counter.

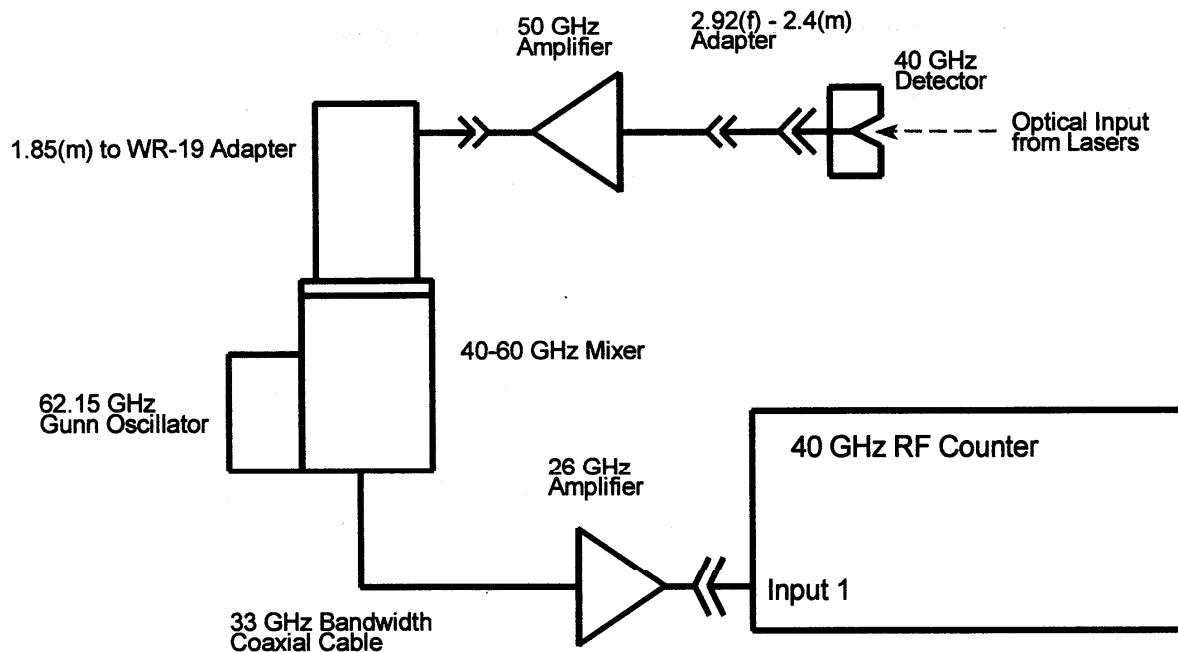


Figure 4. Subassembly for measuring frequency between 40 GHz and 58 GHz. System actually operates down to about 36 GHz.

Three generic types of open loop sweeps can be performed. The first is a scan of up to 40 GHz in 2 parts through a mode-hop. The temperature of both lasers is initially set so that the difference frequency is about 40 GHz. This positions each laser at the extreme end of the temperature range where single-mode operation is possible. YAG2 is then scanned toward the opposite end of its stable region ending with a difference frequency around 18 GHz. YAG3 is then shifted by about 20 GHz, and YAG2 is tuned back to where it started. At this point VBS2 must be manually adjusted to compensate for the changed power from YAG3 that is coupled into the fiber going to the photodiode specimen. We believe that the direction of the beam from YAG3 changes slightly when the laser's temperature changes, causing the power that is coupled into the fiber to change. If YAG2 is ever replaced with a similar new laser, this problem must be corrected. YAG2 is then scanned as before with a starting frequency near 20 GHz and sweeping through dc. When diode power sensors are used, the sweep is usually done too quickly to reliably change input ranges on the counter to measure frequencies below 500 MHz, causing some drop-outs in that region. The finest sample spacing achievable without using an external

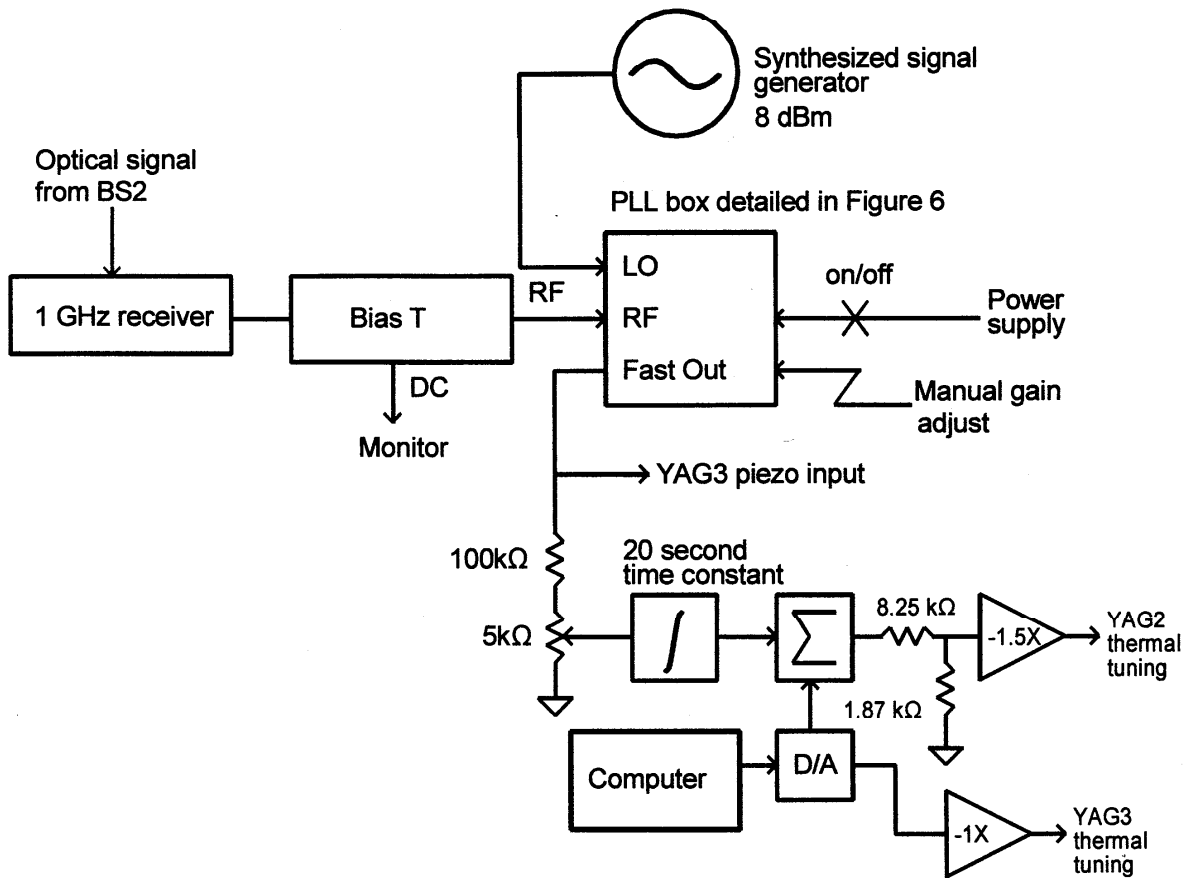


Figure 5. Schematic of circuit for frequency control, including phase-locked operation. Power supply for PLL box is turned off for swept (open loop) operation.

voltage divider is about 5.8 MHz using the 1.5× external amplifier, giving the finest calibration data spacing of about 45 MHz.

The second type of scan is designed for finer resolution scans and can automatically switch between counter inputs to select the correct operating frequency range. YAG3 is left at one position and YAG2 is swept to achieve sample spacing as low as 30 kHz. The finest frequency resolution attainable in an open loop or swept mode can be achieved by attenuating the input to the external amplifiers for YAG2 using the 1.87kΩ/8.25kΩ divider shown in figure 5.

The third type of scan is used for the 40 to 60 GHz band and uses the external mixer with the counter (see figure 4). The measured frequency is corrected for the Gunn oscillator frequency to give the actual optical beat frequency. In this case YAG3 is cooled and YAG2 is swept to achieve sample spacing of about 5 MHz.

A fourth option is a phase-locked mode which steps to specific frequencies. It can synthesize specific frequencies between 10 Hz and 1 GHz. Phase-locked operation is described in the next section.

These scan options are accessible through a user interface program called HETSETUP.BAS. This interface program is designed to be run as an executable which calls other programs, also in compiled executable form, which run the different scan options listed above. The measurement number is recorded in a master file and is incremented with each scan, so that subsequent measurements use a unique file number. A setup file for each calibration records the file numbers that were used for that calibration along with the detector name and type and customer name. Data files generated by the programs described above contain the corresponding setup file name, data file name, temperature, and relative humidity for the scan. The files then split into four columns that contain frequency (in gigahertz), rf power (in decibels with respect to 1 mW), current (in amperes), and normalized response (in decibels).

3.2 Phase-locked operation

Measurements with resolution of about 100 kHz are desired at low frequencies but the minimum practical resolution for swept measurements is greater than 30 kHz, giving the final data spacing of about 300 kHz. A method that gives very fine resolution and solves problems related to scanning the beat frequency through dc is to synthesize the beat frequency between the two lasers using a phase-locked loop. Early work demonstrating phase-locked operation of two nonplanar Nd:YAG lasers operated at low frequencies and displayed small capture ranges. Later work by several authors [12], [13] showed broadband operation above 10 MHz. However, most high bandwidth phase-locking circuits have minimum operating frequencies of a few tens of megahertz and are not suitable at the relatively low frequencies required for some applications. We have solved this problem by generating a secondary optical signal whose frequency is offset from the main signal by 70 MHz (see figure 2). The phase locking electronics then see a signal near 70 MHz when the offset frequency of the main signal is very low.

The electronics for the phase-locked loop (PLL), shown in figure 6, were developed by the Time and Frequency Division at NIST [14], [15]. The local oscillator (LO) is offset from the rf frequency by 15 MHz (see figure 5). The difference frequency between the LO and rf signals is sent to a phase comparator to compare with an inexpensive TTL oscillator operating at 55 MHz, and generates an error signal that is filtered and fed back to the laser frequency control. For the sign of the error signals used the beat frequency f_2 at BS2 is offset from f_1 (at BS1) by 70 MHz and is offset from the LO by 15 MHz. For the main signal at BS1 to have a frequency of 1 MHz, the beat frequency at BS2 is 71 MHz and the LO is set at 16 MHz. The frequency stability is limited by the relative stability of the 55 MHz TTL oscillator, 70 MHz crystal oscillator, and synthesized LO. We have not attempted to stabilize these oscillators relative to each other.

Phase-locked frequency control in our heterodyne system works well between about 300 kHz and 1 GHz. Unfortunately, phase-locked operation below 100 kHz is unstable, probably due to coupling between the laser relaxation oscillations and the phase detection circuit.

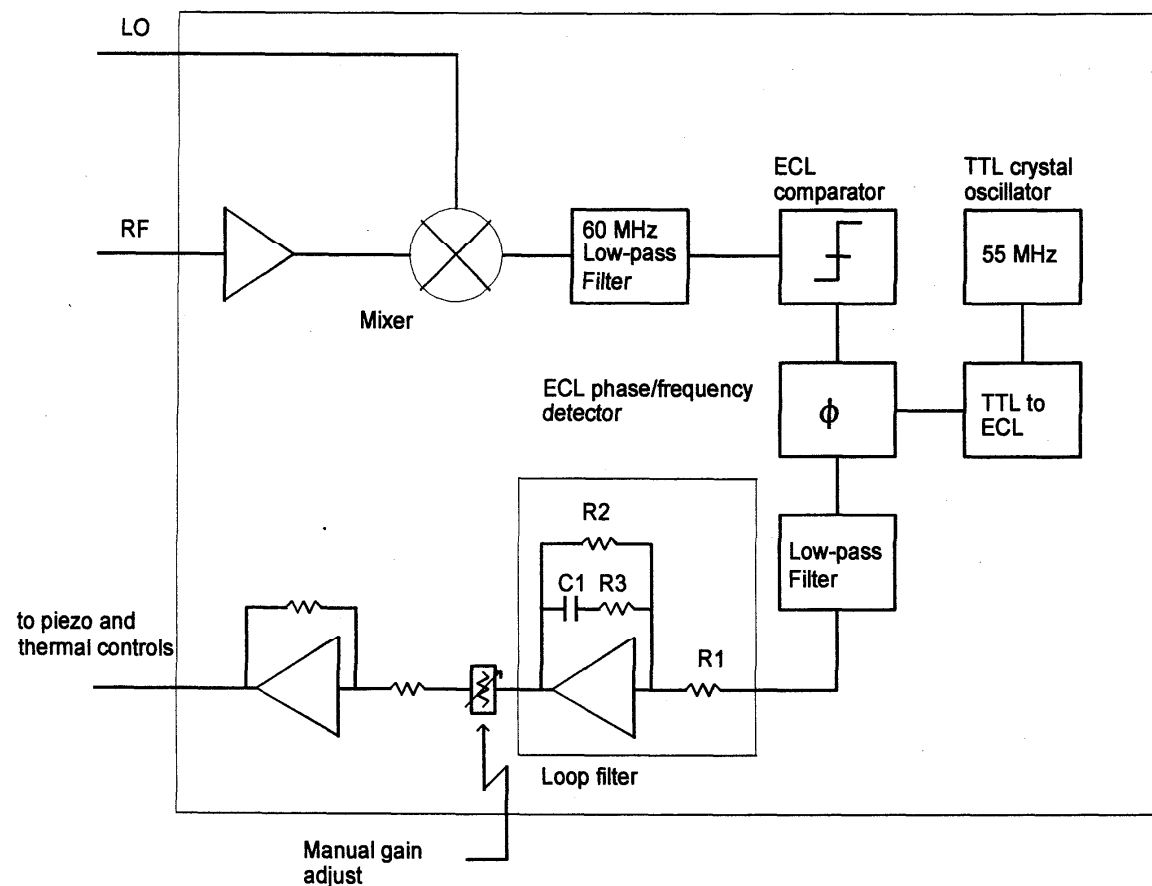


Figure 6. Schematic of PLL box from figure 5. Component values for the loop filter are $R1=137 \Omega$, $R2= 158 \text{ k}\Omega$, $R3= 3 \Omega$, and $C1= 1 \mu\text{F}$.

3.3 Power matching

The NIST heterodyne system is designed to operate with 100 % modulation depth and to use the normalization described by eq (6). Control of the modulation depth is achieved by three features of the system: mode matching of the radiation incident on the detector from each laser, polarization matching, and power matching. Mode matching is achieved by launching the laser beams into roughly 2 m of single mode fiber. Polarization matching is provided by the polarizing isolators. Any birefringence in the optical path following the isolators changes the relative polarization of the two laser signals by a negligible amount. The power from each laser is matched by fine adjustments of variable beam splitters VBS1 and VBS2. Typically, a high power is required for the high speed detector used for frequency measurement, so the ratio of the power

going to the frequency measurement assembly to the power going to the specimen is controlled by VBS3.

Effects which cause the modulation depth to vary from 100 % should be minimized. The optical return loss of test devices should be higher than 20 dB to reduce multipath interference in the fiber delivering light to the detector. Fiber connectors used should mate with minimal gap to avoid wavelength dependence in the insertion loss. Since the power from YAG3 which is coupled into the fiber changes when it is thermally tuned, VBS2 must be used to adjust its power before the second part of a 40 GHz scan.

4. Uncertainty in combined photodiode/power sensor normalized response

Uncertainties in the measurement of a photodiode with a current monitor and a receiver without a current monitor are different. Uncertainties peculiar to a receiver without current monitor will be discussed in Appendix D. Typical uncertainties for the photodiode are listed in table I. [16] Type A uncertainties are uncertainties that can be calculated using purely statistical analysis and include repeatability, offset correction, and reproducibility (environmental effects). Type B uncertainties are inferred by other means. The coverage factor of 2 gives approximately 95 % confidence that the true value of the frequency response lies within the interval [measured value \pm expanded uncertainty] if all the uncertainties obey a Gaussian distribution. We anticipate that most customers who are interested in calibrations of this type will be mostly interested in uncertainties that might change the shape of the frequency response and are not as concerned with the absolute response. The type B uncertainties that are important for this type of transfer standard are quantities which might vary with frequency or which might change during the measurement. Range-scaling uncertainties in the meter are included in the uncertainty budget since the range setting might change during the measurement. The current monitor is also included because its offset may drift. Uncertainties in the 50 MHz calibration standard in the power meter are not usually included, although they are outlined below. A standard that can not be connected to the 50 MHz reference calibrator introduces an arbitrary shift (or scale factor in linear units) that can change between measurements, and which must be corrected. Optical connector repeatability is not an issue in the normalized response measurement since the response is normalized to the dc photocurrent, which is proportional to the power actually hitting the detector. We assume that any insertion loss in the connectors has negligible wavelength dependence. rf power meter range scaling and bias current monitor uncertainties are the dominant contributions to the uncertainty budget. The total uncertainty given in table 1 is the square root of the sum of the squared uncertainties (rss). Details of the uncertainty budget are given below.

4.1 Type A uncertainties

Repeatability: Since the heterodyne system uses a swept measurement, different scans will not repeat exactly the same frequencies, nor will the measured frequencies exactly coincide with the requested frequencies. Two scans are made in both forward and reverse directions, giving a total

Table 1. Summary of typical frequency response measurement uncertainties for photodiode with rf power sensor and 3 dB attenuator.

Source of uncertainty	Uncertainty, $k = 1, \%$
Type A	
Measurement repeatability s	<0.05
Offset correction s_a	0.007
Environment effects s_e (f in GHz)	$0.106 + 0.00064 f + 0.00024 f^2$
Type B	
Meter range scaling	0.5
Meter offset	0.023
Optical power drift (power matching)	0.06
Bias current measurement	0.08
Power sensor noise, @ 0.05 GHz	0.025
@ -3 dB point	0.05
Total uncertainty (rss), @ 0.05 GHz	
@ -3 dB point, 31 GHz, 4 scans	0.63
Expanded uncertainty (coverage factor $k = 2$), @ 0.05 GHz	
@ -3 dB point, 31 GHz, 4 scans	1.25 (0.05 dB)

of four scans over each range. The response and its standard uncertainty at the requested frequencies are found using the following method. Let $\mathbb{R}^2(f)$ be the measured response at frequency f . The calculation is usually performed with $\mathbb{R}^2(f)$ in dB with negligible error because the scatter in the data is small. The response at the requested frequency x is estimated by a kernel-type smoother [17]. Specifically,

$$\tilde{\mathbb{R}}^2(x) = \frac{\sum_{i=1}^n K\left(\frac{x - f_i}{b}\right) \mathbb{R}^2(f_i)}{\sum_{i=1}^n K\left(\frac{x - f_i}{b}\right)}, \quad (9)$$

where b is the bandwidth parameter and $K(\cdot)$ is the kernel function, which typically has the following properties:

1. $K(\xi) \geq 0$ for all ξ
2. $\int_{-\infty}^{\infty} K(\xi) d\xi = 1$ (10)
3. $K(-\xi) = K(\xi)$ for all ξ .

That is, $\tilde{\mathbb{R}}^2(x)$ is obtained as a weighted average of frequency responses around x . The kernel function assigns the weight to each point, and the bandwidth b determines the size of the region around x for which $\mathbb{R}^2(f_i)$ receives relatively large weights. Frequently used kernels include rectangle, triangle, and Gaussian functions. The rectangular kernel assigns equal weight to the points inside the rectangle and ignores the points outside. Both the triangle and Gaussian kernel assign the most weight to the points that are closer to x . In our applications, we use the Gaussian kernel

$$K(\xi) = \frac{1}{0.37\sqrt{2\pi}} e^{-\frac{\xi^2}{2(0.37)^2}} \quad (11)$$

The kernel is scaled to have 25th percentile of -0.25 and a 75th percentile of 0.25 .

Many methods have been proposed for bandwidth selection.[18] In practice, b can be determined by the average frequency increment in the scan, and the desired number of points

used to calculate $\tilde{\mathbb{R}}^2(x)$. For example, if the Gaussian kernel is used, the average frequency increment is h , and roughly p points on each side of x are to be included; that is, $|x - f_i| \leq ph$. Any point with $|(x - f_i)/b| > 1$ receives almost 0 weight; that is, we want $|(x - f_i)/b| \leq 1$ or $b \approx ph$. The “resolution” of the measurement is then about $0.37ph$. We typically take data so that the spacing between acquired points is 0.1 to 0.2 times the final data spacing (resolution) required. We then use $p = 2$ giving an approximate resolution of 0.07 to 0.14 times the customer’s requested frequency spacing.

The kernel-smoothing technique, like all other smoothing techniques, has an error associated with it. This error is small when the response is roughly linear with frequency, but may become significant in regions with large curvature. The approximate mean-squared error of the kernel

estimator $\tilde{\mathbb{R}}^2(x)$ is given by [19]

$$MSE(x) = 0.004 \ 685 \ b^4 \ c_x^2 + \frac{0.762 \ 42 \ \sigma^2}{nb}, \quad (12)$$

where c_x is the second derivative of $\mathbb{R}^2(y)$ evaluated at $y = x$ using a spline method and σ^2 is the variance of the response of a given scan. This variance, however, is unknown and needs to be estimated. A technique [20] that works well and can be used to obtain an estimate of σ^2 is to “detrrend” the data locally and use the sample variance of the detrended data. The detrended residual value at f_i is defined as

$$r_i = \mathbb{R}^2(f_i) - \frac{\mathbb{R}^2(f_{i+1}) + \mathbb{R}^2(f_{i-1})}{2} \quad (13)$$

and the variance estimator is found by

$$\hat{\sigma}^2 = \frac{2}{3(n-2)} \sum_{i=2}^{n-1} r_i^2. \quad (14)$$

Let $\tilde{\mathbb{R}}_i^2(x)$ and $MSE_i(x)$ be the estimated response and the mean-squared error at frequency x of the i th scan. The estimated mean response based on m scans is

$$\overline{\mathbb{R}^2}(x) = \sum_{i=1}^m \frac{\tilde{\mathbb{R}}_i^2(x)}{m}, \quad (15)$$

and its standard error is

$$s(x) = \sqrt{\frac{s_b^2(x) + s_w^2(x)}{m}}, \quad (16)$$

where

$$s_b(x) = \sqrt{\sum_{i=1}^m \frac{(\tilde{\mathbb{R}}_i^2(x) - \overline{\mathbb{R}^2}(x))^2}{m-1}} \quad (17)$$

is the between-scan uncertainty and

$$s_w^2(x) = \sum_{i=1}^m \frac{MSE_i(x)}{m} \quad (18)$$

is the uncertainty within a scan due to kernel smoothing. Repeatability is a function of the rf connector type, frequency, electrical mismatch, and other factors that cannot be controlled.

Other smoothing techniques can also be used, in particular, spline methods. We did not use a spline method to interpolate the measurements because spline methods give unsatisfactory results near the end points, use arbitrary knot spacing, and give a poorly defined resolution. In addition, the splines over-smooth the peaks and valleys. For example, the dots in figure 7 represent the measured response, \square denotes the interpolated responses at requested frequencies based on a cubic spline fit, and \times denotes the interpolated responses at requested frequencies based on the Gaussian kernel smoother. In most cases, both methods agree well, but clearly the spline method gives poorer results in the neighborhood of 23.5 GHz. Uncertainty due to the kernel smoothing is negligible on most detectors that we have calibrated; for example, $s_w \leq 0.002$ dB for the data in figure 6.

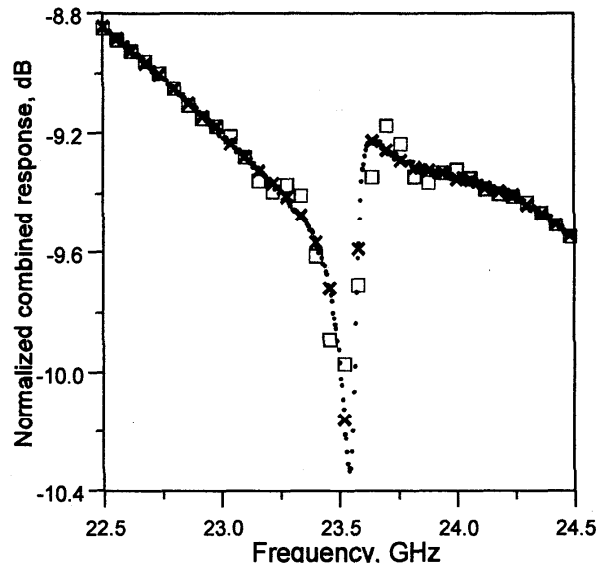


Figure 7. Dots represent the measured response, \square denotes the interpolated responses at requested frequencies based on a cubic spline fit, and \times denotes the Gaussian kernel smoother.

Offset correction: When the power sensor gain is not scaled to the 50 MHz power reference (or when the frequency response is normalized to the optical power instead of the photocurrent), a correction due to the scale factor must be included. The scale factor (offset on a logarithmic scale) is constant for each scan and does not have a frequency dependence if coherent multipath effects are insignificant. The fiber connector insertion loss repeatability is typically about 0.1 dB and is larger than other uncertainties in the measurement. Variation in the scale factor is normally about 0.005 dB. However, if the meter is used with a different power sensor and it is scaled relative to the 50 MHz reference, the scale factor could change by a few tenths of a decibel. Also, scans over the low and high frequency ranges are often made separately and with different data spacing, so a method for "splicing" the two overlapping frequency ranges is required. This is accomplished by shifting all the scans to a common level (on a logarithmic scale) selected by a least-median technique. Using this technique, the individual scans are shifted by averaging over all desired frequencies where scans overlap. The entire data set is then normalized to give 0 dB at some frequency, typically 50 MHz. The absolute response then has a

relatively large uncertainty, while the shape is specified with much lower uncertainty. The technique described below is valid for logarithmic data if the offsets or outliers are less than a few tenths of a decibel; otherwise, the calculation should be performed with responsivity in linear units. If this were the case, the procedure below would need to be modified to accommodate a linear scale factor instead of a shift.

If there are m scans over n_0 overlapping frequencies f_i , then offset adjustment factors can be calculated by minimizing the expression

$$\sum_{i=1}^{n_0} d(\tilde{\gamma}_1(f_i) - a_1, \tilde{\gamma}_2(f_i) - a_2, \dots, \tilde{\gamma}_m(f_i) - a_m), \quad (19)$$

where $d(\cdot, \cdot, \dots, \cdot)$ is an "appropriate" distance metric and $\tilde{\gamma}_m = 10\log(\tilde{R}_m^2)$ or $10\log(\tilde{g}_m^2)$, as appropriate for the particular measurement (see Appendices A and D for definition of g). A possible metric for our application is absolute deviation from the mean. Let

$$\bar{\gamma}(f_i) = \sum_{j=1}^m \frac{\tilde{\gamma}_j(f_i)}{m} \quad (20)$$

be the mean response at f_i and define the distance metric as the sum of the distance (absolute difference) between $\tilde{\gamma}_j(f_i) - a_j$ and the mean response $\bar{\gamma}(f_i)$

$$d(\tilde{\gamma}_1(f_i) - a_1, \dots, \tilde{\gamma}_m(f_i) - a_m) = \sum_{j=1}^m |\tilde{\gamma}_j(f_i) - a_j - \bar{\gamma}(f_i)|. \quad (21)$$

The expression we need to minimize is

$$\sum_{j=1}^m \sum_{i=1}^{n_0} |\tilde{\gamma}_j(f_i) - a_j - \bar{\gamma}(f_i)|. \quad (22)$$

Given the sequence y_1, y_2, \dots, y_k the value of a that minimizes

$$\sum_{i=1}^k |y_i - a| \quad (23)$$

is $a = \text{median of } y_1, y_2, \dots, y_k$. Thus the solution for a_j is that a_j is the median of

$$\tilde{\gamma}_j(f_1) - \bar{\gamma}(f_1), \tilde{\gamma}_j(f_2) - \bar{\gamma}(f_2), \dots, \tilde{\gamma}_j(f_{n_0}) - \bar{\gamma}(f_{n_0}). \quad (24)$$

The offset uncertainty can be characterized by the standard deviation of the a_j . If y_1, y_2, \dots, y_k are independent Gaussian random variables, the variance of the median of y_1, y_2, \dots, y_k is approximately equal to [21]

$$\frac{\pi \text{var}(y_i)}{2k} \quad (25)$$

Now, by expanding $\bar{y}(f_i)$ into a sum, we can show that

$$\text{var}(\tilde{y}_j(f_i) - \bar{y}(f_i)) = \frac{m-1}{m} \text{var}(\tilde{y}_j(f_i)) \quad (26)$$

so an estimate of the variance of a_j is given by

$$s_{a_j}^2 = \frac{(m-1)\pi\delta^2}{2mn_0} \quad (27)$$

where δ^2 is the variance estimate of scan j given in eq (14).

Environmental conditions: Another source of uncertainty is due to environmental conditions such as temperature, pressure, relative humidity, and other unknown interfering factors. A check standard was constructed in an attempt to evaluate these effects and to track changes in the measurement system. Unfortunately, each transfer standard is affected by these parameters differently, and it is impossible to evaluate the long term reproducibility or stability of each customer's transfer standard. We intend that our measurements of the check standard to be used as a measure of the system reproducibility and that the reproducibility of the transfer standard be left to the customer.

The check standard consists of two photodiodes, each with regulated bias and bias monitor circuits. The photodiode labeled "Lowband" has a nominal bandwidth of about 16 GHz and is connected to a 3 dB attenuator, a 3.5 mm to N adapter, and a commercial rf power sensor (diode) that operates between 100 kHz and 4.2 GHz. The photodiode labeled "Highband" has a nominal bandwidth of about 30 GHz and is connected to a 3 dB attenuator and a commercial rf power sensor (diode) that operates between 50 MHz and 50 GHz. Both photodiode assemblies are permanently mounted in a box with a power supply and access to the bias monitor and power sensor. Measurements were made on both bands over a year's time. Because the photodiodes were permanently joined with the power sensor, no connection to the 50 MHz reference source on the power meter could be made. Hence all measurements were simply normalized to the value at 50 MHz. The nominal response curves and deviation from the mean are shown in figures 8 through 10.

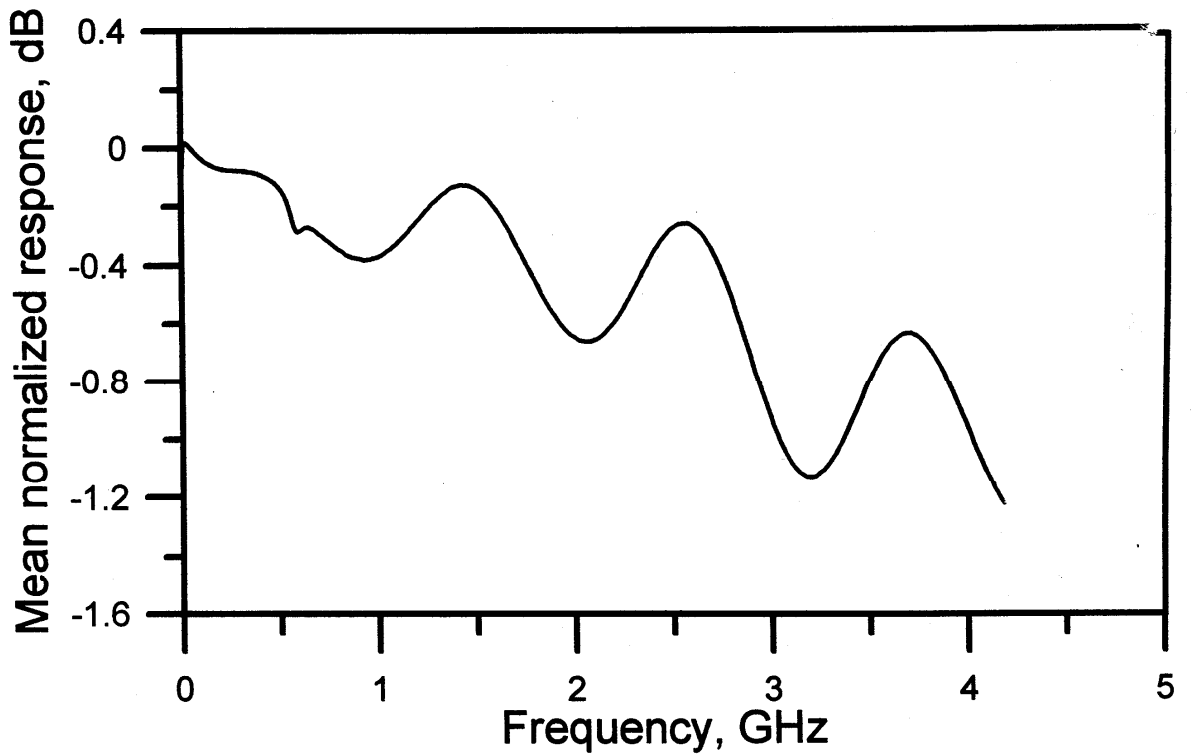
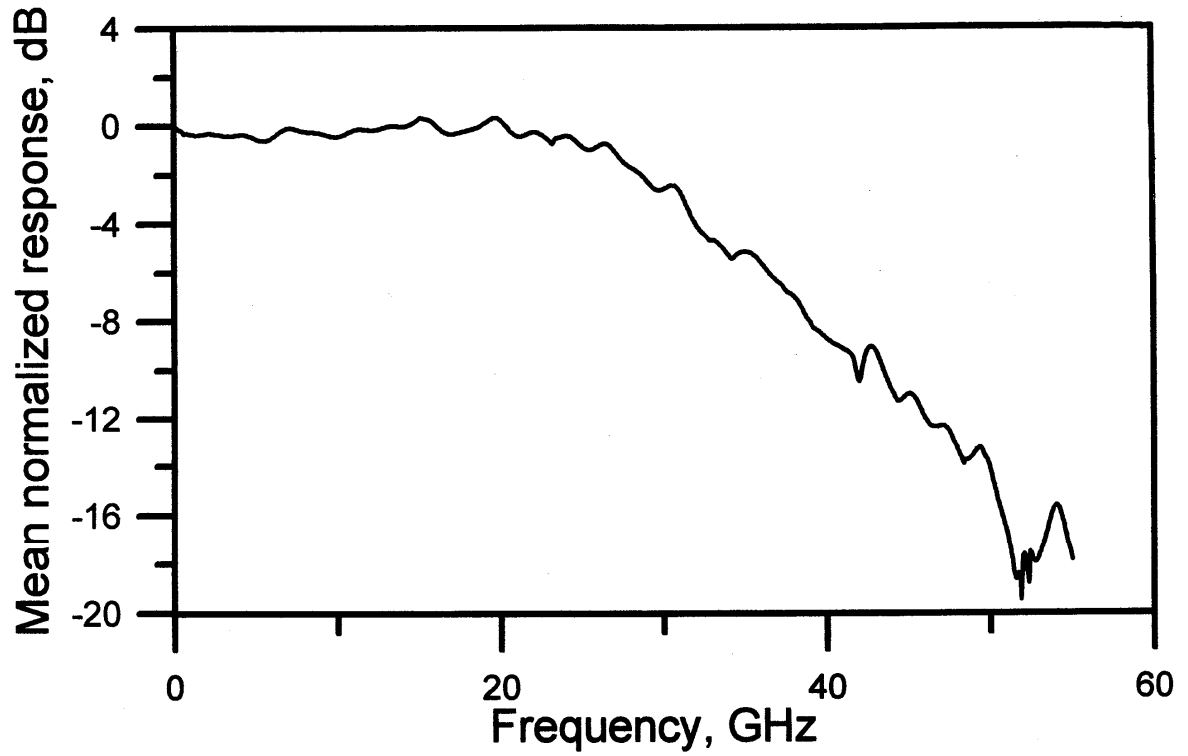


Figure 8. Mean normalized response of the check standard shifted to give 0 dB at 0.05 GHz. Upper graph is highband, and lower graph is lowband.

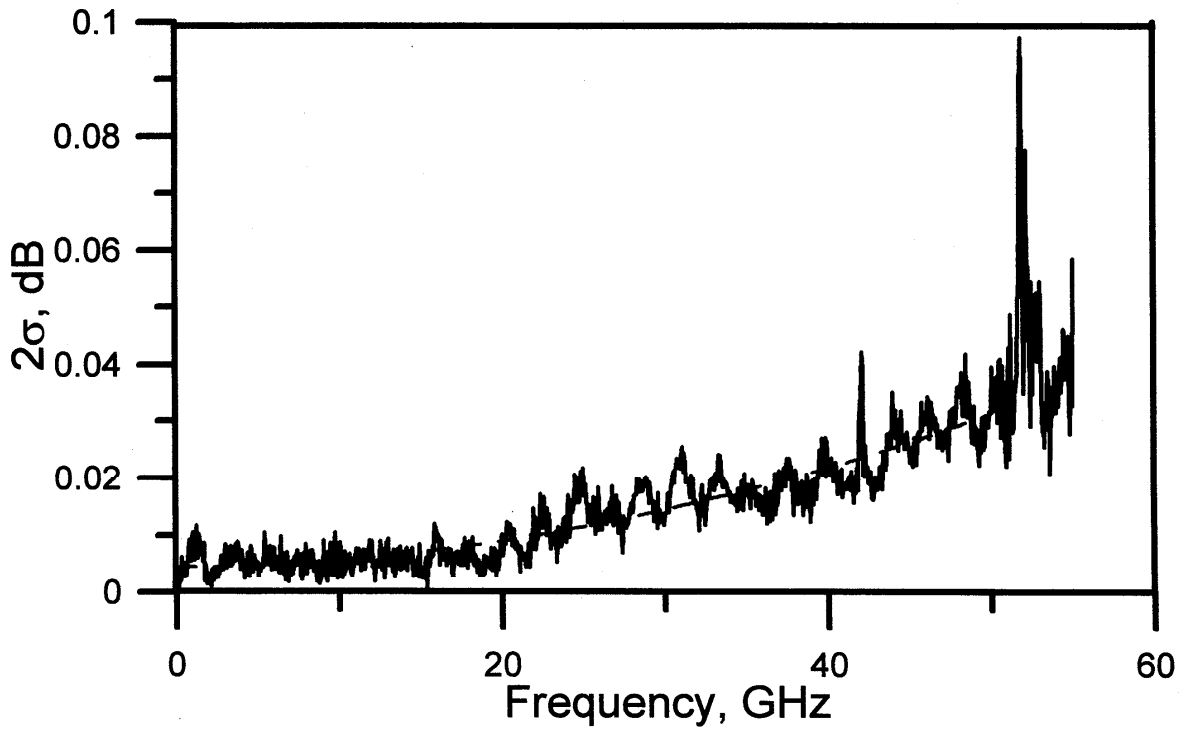
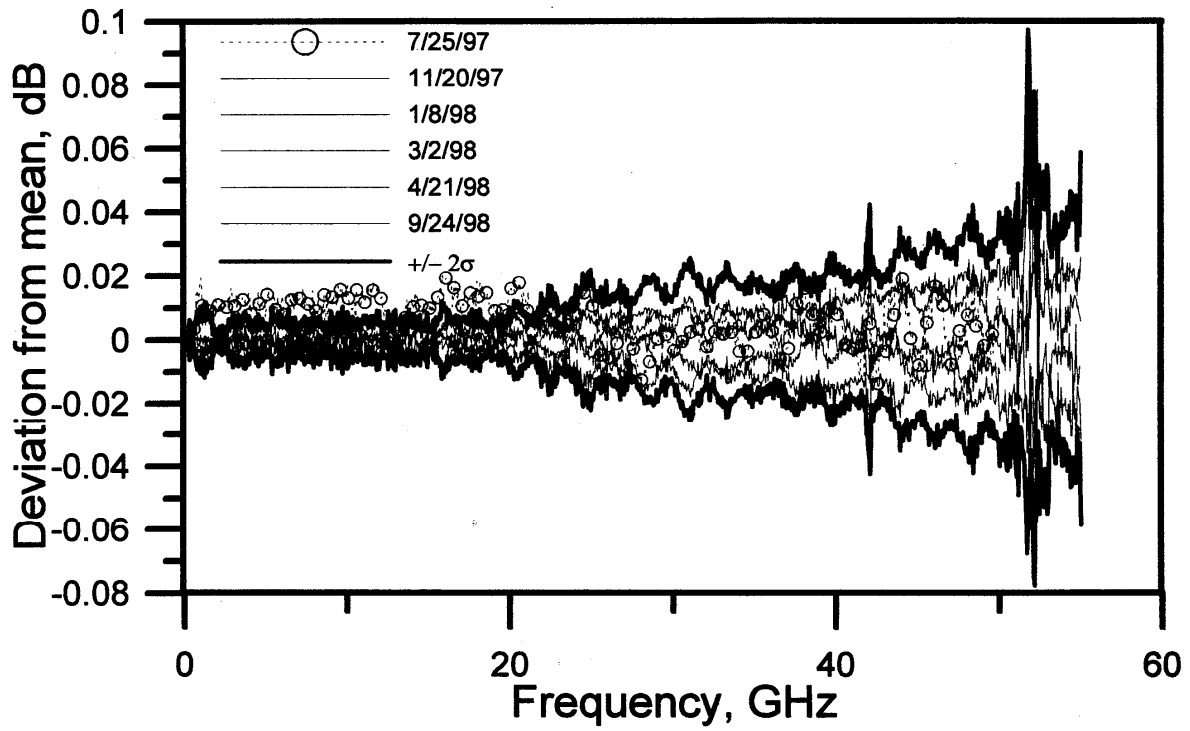


Figure 9. Measurements on highband of the check standard. Top graph shows deviation from the mean which neglects measurements on July 25, 1997. Bottom graph shows the 2σ variation with a fit to a quadratic equation. Spikes at 52 GHz go out of the range of the graphs.

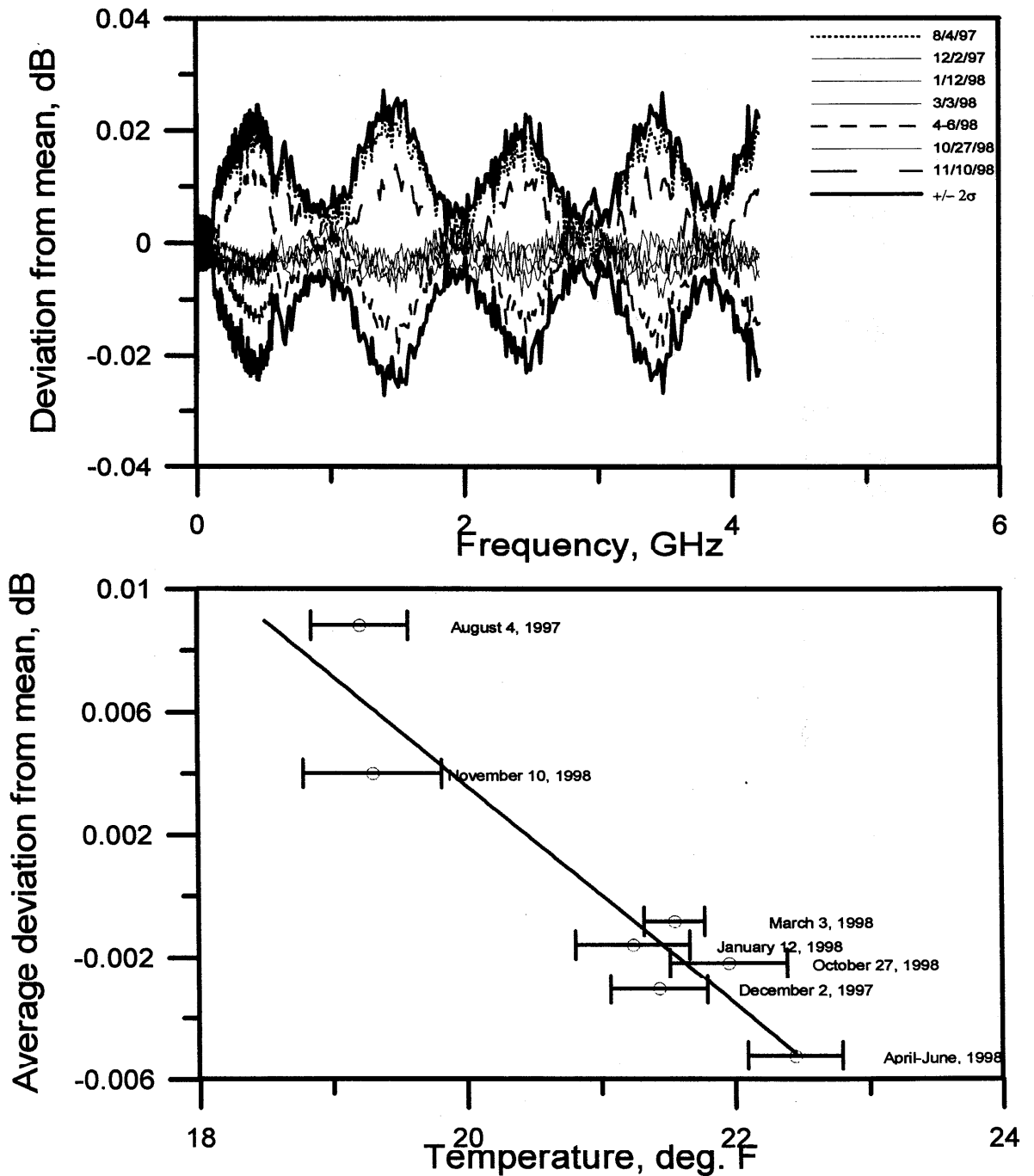


Figure 10. Top graph shows the deviation from mean of measurements on the check standard lowband. Influence of measurements made 8/4/97, 4-6/98, and 11/10/98 is clearly seen. When these data sets are dropped, 2σ is about 0.05 dB. Bottom graph shows correlation between temperature and average offset from mean of data sets. Error bars are one standard deviation of the data and do not include inaccuracy of the thermometer.

Measurements on the highband photodiode consisted of swept scans over the following approximate ranges: 50 MHz to 1 GHz, 500 MHz to 40 GHz, and 38 GHz to 55 GHz. Two scans were made in both forward and reverse directions, giving a total of four scans in each range. The room temperature and relative humidity were measured before each scan. Where scans overlap in frequency, the lower frequency scan was always used in the final analysis. A plot of the deviation from the mean (see figure 9) shows monotonically increasing uncertainty with frequency with large spikes near 43 and 52 GHz where the frequency response of the standard has notches. There is not a jump in the deviation in the region of 40 GHz, where frequency is measured with the Gunn oscillator and mixer, showing that frequency accuracy is not a major problem in the 40 to 55 GHz region, although this may be part of the reason for large uncertainties at the notches at 43 and 52 GHz. The measurement performed on July 25, 1997, shows a significantly higher deviation than the other scans below 23 GHz, but then is in the middle at higher frequencies. If this data set is neglected, the 1σ deviation from the mean fits roughly a second-order polynomial in frequency,

$$s_e(f) = a_0 + a_1 f + a_2 f^2 . \quad (28)$$

Measurements on the lowband photodiode consist of a swept scan over the range of a few megahertz to 4.2 GHz and a set of data acquired using the phase-locked loop between 300 kHz and 600 MHz. Swept measurements were made in the forward and reverse directions giving a total of four scans and three sets of data were acquired using the phase-locked loop. A plot of the deviation from the mean (see figure 10) shows that measurements taken on August 28, 1997, fall above the mean and measurements in April/June 1998 fall below the mean. Both data sets have a large ripple indicating that the ripple in the frequency response was distorted in these measurements. In an attempt to find a correlation between room temperature and these deviations, the average temperature was plotted against the average deviation for each data set showing a possible trend. A final measurement taken November 10, 1998, with the room temperature intentionally lowered appears to confirm the trend. Whether this trend is the cause of the slightly higher value in the data below 23 GHz in the highband data is unknown.

Since the lowband data for August 28, 1997, and April/June 1998 were shown above to be outliers, they can be discarded. Then the data from the lowband measurements and highband measurements are consistent and the expression for the environmental random variation in eq (28) is still valid if the laboratory temperature stays at 21.55 ± 0.28 °C. It is possible that environmental uncertainty is mostly due to environmental effects on the check standard and not on the measurement system. However the check standard is the most stable device that we have been able to construct, and its stability cannot be measured independently from the stability of the measurement system. Until a better check standard is available, the reproducibility of the check standard measurements will be used as a measure of the system stability. This is a good assumption since the contribution of s_e is not really significant below about 40 GHz. The combined type A uncertainty is then found by adding the components of uncertainty in quadrature [14]. That is, we use

$$s_A = \sqrt{s^2 + \frac{s_a^2}{m} + s_e^2} \quad (29)$$

as the total type A uncertainty in Table 1, s^2 is obtained using the offset adjusted data in eq (16), m is the number of scans within the particular frequency band, and s_a^2 is the maximum of the $s_{a_j}^2$ (see eq (27)) for all the scans and frequency bands. If offsets are not required $s_a = 0$.

4.2 Type B uncertainties

Meter range scaling: This uncertainty is due to the inaccuracy of the gain for different power ranges. The absolute accuracy of the power meter is specified by the manufacturer as 0.5 % and is assumed to be 1σ . This is conservative; if the specified uncertainty were actually 2σ the estimated calibration uncertainty would be reduced. Also, the uncertainty is assumed to obey a Gaussian distribution instead of rectangular distribution. This is also a conservative assumption. The meter range scaling uncertainty is the dominant contribution to the uncertainty budget in Table 1.

Meter offset: The settability of the zero level, specified as one least significant count on the display or 0.001 dB (0.023 %), is assumed to be 1σ . Additional zero setting error is 0.5 % of full scale deviation of lowest range. For the diode power sensor this is 5 pW.

Optical power drift (power matching): Power from one or both of the lasers that is coupled into the fiber may drift during the measurement. Also because of the long coherence length of the Nd:YAG laser, multipath effects cause the power matching between the two lasers to vary with frequency. The power from each laser does not drift by more than 4 %, giving a 0.04 % uncertainty in the ratio of eq (6). This quantity is assumed to be 1σ for one of the lasers. Adding the uncertainty in quadrature for two lasers gives ± 0.06 % uncertainty.

Bias current measurement: The scale factor in the current monitor used in the check standard has a temperature coefficient of about 0.14 %/°C. Using the laboratory drift of about ± 0.28 °C, the uncertainty in the bias current is 0.04 %. Squaring gives a 0.08 % uncertainty in the normalized response. If a bias current monitor is not provided, the voltage drop across a 1 k Ω resistor in series with the detector is measured. The temperature coefficient of the resistor is 0.01 %/°C giving 0.0028 % uncertainty. The specified accuracy of the voltmeter on the 300 mV range is 0.0025 %, which is assumed to be 1σ . Other current monitor circuits may have different uncertainties. The dark current and/or offset of the monitor circuit is subtracted from the measured current.

Power sensor noise: This is the uncertainty associated with the background noise of the detector, which is about -75 dB (re: 1 mW) for the diode power sensor. Using 100 μ A total

bias current and a 3 dB pad gives an error of 0.013 % at low frequencies. The background noise is about -40 dB (re 1 mW) for thermal power sensors.

Reference power uncertainty: If the transfer standard is of the type where the power sensor is to be disconnected to scale the power meter gain, an uncertainty from the 50 MHz reference source needs to be included, since it is assumed that the intent of the sensor is to calculate absolute modulation depth. The power reference accuracy is specified by the manufacturer as $\pm 0.9\%$ RSS for one year and is assumed to be 1σ . Mismatch between the power sensor and the reference gives an additional error. The reference is specified as having a maximum VSWR of 1.05, giving $\rho \leq 0.024$. The reflection coefficient of the power sensor at 50 MHz typically varies between 0.015 and 0.03. An upper bound for the mismatch error is $|1 \pm (0.024)(0.03)|^2 - 1 = \pm 0.0014$, or $\pm 0.14\%$. Modeling the distribution as uniform, gives a standard deviation of 0.08 %.

Gunn oscillator frequency drift: Uncertainty in the normalized response due to frequency drift is given to first order by

$$\delta(10\log[\mathfrak{R}^2(f)]) = \delta f \cdot \text{slope}. \quad (30)$$

A maximum slope is about 3 dB/GHz, the drift of the oscillator is about 9 MHz/°C and the laboratory temperature drift is about ± 0.28 °C worst-case. This gives an uncertainty in the normalized response of about 0.008 dB or 0.17 %.

Hysteresis: Averaging internal to the power meter can cause the meter response to effectively shift and smooth sharp features in the frequency response. This is avoided by using 0.01 dB resolution, with the default averaging factor instead of 0.001 dB resolution and making two scans in both forward and reverse directions. The result of scanning in opposite directions is to (a) average errors and (b) flag regions where there are problems by showing large interscan uncertainty.

Relative intensity noise: Laser relative intensity noise (RIN) could degrade the accuracy of the heterodyne measurement system by adding a small amount of power to the measurement from both the spontaneous-spontaneous beat note and the signal-spontaneous beat note. In the Nd:YAG system, the signal-spontaneous beat noise causes side lobes are >30 dB (re: carrier) below the carrier at about 100 kHz offset. This places a small error on the resolution of the system, but this error is insignificant for most real detectors. The spontaneous-spontaneous beat noise is many orders of magnitude lower and is an insignificant source of error.

5. Quality Control

5.1 Calibration notebook

A notebook which describes the measurement setup for all calibrations, voltage range range used for each scan and corresponding frequency range, biasing conditions, adapters, and any other pertinent information will be kept.

5.2 Checks on each calibration

A system failure which would possibly give erroneous results occurs when the lasers are not truly operating in a single mode. This is the usual problem in laser temperature regions where the laser mode is unstable and near a mode hop. A spurious mode has also been observed in YAG3 for certain tuning conditions. Precautions which will be taken to ensure rejection of invalid data due to spurious modes include checking the optical spectrum analyzer at the beginning and occasionally during a scan.

Frequency scans over adjacent bands should overlap both in frequency and in magnitude. Typical offset between scans is less than 0.02 dB. If the bands do not overlap, and the power meter scale factor was not set with a different power sensor, then the operator should search for the cause of the problem.

The bias current for each scan will be checked and should change by no more than 5.6 %.

5.3 Periodic checks

Power stability: When the data for a scan are being acquired, the total photocurrent is monitored and during the analysis of the data it is checked to make sure it did not vary out of the specified 5.6 % (1σ) total allowed deviation. However, periodically, the photocurrent of the each laser will be monitored during a frequency scan to check for problems.

Gunn oscillator frequency: The frequency of the Gunn oscillator used for downconverting frequencies in the 40 to 60 GHz band is subject to change with temperature and external stresses, such as from mounting clamps. The frequency and temperature dependence of the Gunn oscillator will be checked periodically or after major changes to its mount. This is accomplished by mixing the oscillator's signal with a source of known frequency near 50 GHz and measuring the difference frequency.

Check standards: A check standard is used to verify the operation of the heterodyne system. A fixed reference standard has been implemented (designated NIST ET) and is described in the section on environment sources of uncertainty above. Periodic measurements on this standard will be performed to verify the system integrity and to obtain better information on the check

standard itself. As further measurements on the check standard are acquired, the estimate of s_c will be modified.

5.4 Future system changes

Possible future system changes could include, but are not limited to, replacement of YAG2, modification of YAG3, use of an electrical spectrum analyzer for frequency measurement, use of an additional laser for extending the frequency range above 60 GHz, replacement of the 40 GHz bandwidth detector, or corrections for system "bugs." Future system changes will be documented in a calibrations notebook which will be kept with the system. Instructions which are specific to the NIST heterodyne system and data analysis are also kept with the system.

5.5 Transfer standards which are suitable for calibration

The transfer standards must include a connectorized single-mode input fiber. The fiber connector should be clean and scratch free. The photodiode response should be free of sharp features to minimize calibration uncertainty. The photodiode must have either direct access to the bias point or have an internal current monitor circuit which is stable so that correct normalization can be achieved during each measurement scan. Coaxial rf connectors must be of a precision type, free of debris and in good condition. The power sensor must mate with a power meter which can be controlled via a standard GPIB interface. Depending on the make and model of the power meter used, the customer may be asked to include the power meter with the transfer standard for calibration. Transfer standards which are determined by NIST to not meet these requirements will be returned at the customers expense and will be charged for any labor which may have been required at NIST to determine the suitability of the transfer standard.

6. References

1. *Optical interfaces for equipments and systems relating to the synchronous digital hierarchy.* CCITT (now ITU-TS) recommendation G.957, Geneva; 1990.
2. In this work, all ratios are stated in decibels electrical, that is, $20\log(A_2/A_1)$ where A is a voltage or current. Absolute powers are stated with the reference level, such as -10 dB (re: 1 mW) instead of -10 dBm as suggested in *Letter symbols to be used in electrical technology, Part 3: Logarithmic quantities and units*, IEC 27-3, Geneva; 1989.
3. Valdmanis, J. A.; Rudd, J. V. High-speed optical signals demand quick response. *Laser Focus World*, pp. 141-147; Mar. 1995.
4. Humphreys, D. A.; Lynch, T.; Wake, D.; Parker, D.; Park, C. A.; Kawanishi, S.; McClendon, M.; Hernday, P.; Schlafer, J.; Gnauck, A. H.; Raybon, G.; Hawkins, R. T.; Jones, M. D.; Goll, J. H. Summary of results from an international high-speed photodiode bandwidth measurement intercomparison. Digest, Optical Fibre Measurements Conference, York, U. K., pp. 69-72; 1991.

5. Gifford, A. D.; Humphreys, D. A.; Hale, P. D. Comparison of photodiode frequency response measurements to 40 GHz between NPL and NIST. *Electron. Lett.*, vol. 31, pp. 397-398; 1995.
6. Hale, P. D.; Franzen, D. L. Accurate characterization of high speed photodetectors. *Proc. SPIE*, vol. 2022, pp. 218-227; 1993.
7. Bowers, J. E.; Burrus, C. A. Ultrawide-band long-wavelength p-i-n photodetectors. *J. Lightwave Technol.*, vol. 5, pp. 1339-1350; 1987.
8. Wangsness, R. K. *Electromagnetic Fields*. New York: John Wiley & Sons; pp. 440-443; 1979.
9. *Fundamentals of rf and microwave power measurements*, Hewlett-Packard Application Note 64-1A; 1997.
10. Wong, B.; Kosiorska, H. Factory measurement solutions to predictable field performance of single mode fiber optic connectors. Day, G. W.; Franzen, D. L eds. Technical digest-Symposium on optical fiber measurements; 1992. Natl. Inst. Stand. (U. S.) Technol. Spec. Publ. 839; pp. 23-28; 1992.
11. Gallawa, R. L.; Li, X. Calibration of optical fiber power meters: the effect of connectors. *Appl. Opt.*, vol. 26, pp. 1170-1174; 1987.
12. Kazovsky, L. G.; Atlas, D. A. A 1320-nm experimental optical phase-locked loop: performance investigation and PSK homodyne experiments at 140 Mb/s and 2 Gb/s. *J. Lightwave Technol.* vol. 8, pp. 1414-1425; 1990.
13. Williams, K. J.; Goldberg, L.; Esman, R. D.; Daagenais, M.; Weller, J. F. 6-34 GHz offset phase-locking of Nd:YAG 1319 nonplanar ring lasers. *Electron. Lett.* vol. 25, pp. 1242-1243; 1989.
14. D'Evelyn, L.; Hollberg, L.; PoPovic, Z. B. A CPW phase-locked loop for diode-laser stabilization. *IEEE MTT-S Int. Symposium Digest*, San Diego, pp. 65-68; May 1994.
15. D'Evelyn, L. *Noise characterization of extended-cavity diode lasers using a new phase-locked loop for diode laser stabilization*. M.S. Dissertation, University of Colorado, Electrical and Computer Engineering Dept.; 1994.
16. *Guide to the expression of uncertainty in measurement*. ISO, Geneva; 1993.
17. Silverman, B. W. *Density estimation for statistics and data analysis*. London: Chapman and Hall, pp. 34-72; 1986.

18. Härdle, W. *Smoothing techniques with implementation in statistics*. New York: Springer-Verlag, 1991.
19. Altman, N. S. An introduction to kernel and nearest-neighbor nonparametric regression. *Am. Statistician*, vol. 46, pp. 175-185; 1992.
20. Rice, J. Bandwidth choice for nonparametric regression. *Ann. Statistics*, vol. 12, pp. 1215-1230; 1984.
21. Mood, A. M.; Graybill, F. A.; Boes, D. C. *Intoduction to the theory of statistics*. New York: McGraw-Hill; p. 257; 1974.

Appendix A: Use of transfer standard in a ratio system

A.1 Application of heterodyne formalism to arbitrary modulation depth

Signals that do not have 100 % modulation depth are commonly used in optoelectronic test equipment. An arbitrary modulation depth can be synthesized by varying one or both of the laser powers in the heterodyne system and can be modeled using the same formalism as section 2.1 above. The resulting equations are applicable to any source with an arbitrary modulation depth, such as a laser with direct or external modulation. A notationally simple way to change the model is to let P_{avg} denote the total average optical power incident on the detector, $P_{O1} = \alpha P_{avg}$, and $P_{O2} = (1 - \alpha)P_{avg}$. Then the total optical signal incident on the photodiode is

$$P(t) = P_{avg} + 2P_{avg}\sqrt{\alpha(1 - \alpha)} \cos(2\pi ft) . \quad (A1)$$

The average optical power is then P_{avg} and the absolute modulation depth is $4P_{avg}[\alpha(1 - \alpha)]^{1/2}$, or, in fractional units, the fractional modulation depth M_O is

$$M_O = \frac{P_{max} - P_{min}}{2P_{avg}} = 2\sqrt{\alpha(1 - \alpha)} , \quad (A2)$$

where P_{max} and P_{min} are the maximum and minimum optical powers incident on the receiver. The mean squared currents in the photodiode are

$$\langle i_{dc}^2 \rangle = P_{avg}^2 R^2(0) \quad (A3)$$

and

$$\langle i_{rf}^2 \rangle = 2P_{avg}^2 \alpha(1 - \alpha) R^2(\omega) , \quad (A4)$$

so the ratio of the powers is

$$\frac{2P_{rf}}{\langle i_{dc}^2 \rangle R_L} = M_O^2 \mathfrak{R}^2(f) . \quad (A5)$$

Hence, the modulation depth of an arbitrary source can be measured with a detector of known normalized response. The combined normalized response can be used in eq (A5) if P_m is used instead of P_{rf} . If the normalized response is only known to within a constant scale factor, the modulation depth is known only within a scale factor. This is the case if the photodetector and rf

power sensor are permanently attached and the combined normalized response is further normalized to give 0 dB at 50 MHz.

In the case of the receiver without access to bias current (see Appendix D), the modulation depth of an unknown source can be found in terms of the measured rf power, average optical power, and known voltage frequency response as

$$M_O^2 = \frac{2R_L P_{rf}}{G^2(f) P_{avg}^2} \quad (\text{A6})$$

A.2 Calibration transfer using ratio of measurements

The fundamental problem in making photodetector frequency response measurements is getting accurate knowledge of the modulation depth of the source. The modulation depth of the heterodyne beat signal is known from fundamental principles, but the modulation depth of a directly modulated laser diode is not. The modulation depth of a Mach-Zehnder modulator can be measured, but careful control of bias and net optical transmission are required for accurate measurements. A transfer standard calibrated using the heterodyne techniques described above and the ratio measurement system shown in figure A1 can be used to obtain accurate knowledge of the modulation depth of these sources. The ratio system consists of a modulated light source with unknown modulation depth and a 1×2 coupler. The coupling ratio does not need to be specified. The signal from the coupler is delivered to a DUT and to a reference photodiode attached to a rf power sensor. The modulation depth of the source can be calculated using eq (35) and the known frequency response of the transfer standard photodiode. Then the frequency response of the DUT is

$$\mathfrak{R}_{DUT}^2(f) = \left[\frac{1}{M_O^2} \right] \frac{P_{rf,DUT}}{0.5 \langle i_{dc,DUT}^2 \rangle R_L} \quad (\text{A7})$$

Calculation of the DUT's frequency response this way includes calibration uncertainty of both the power sensors used to measure P_{rf} from the standard detector at NIST and at the customer's laboratory, giving a total expanded uncertainty of 0.2 dB or more for the modulation transfer function. Combined with other factory uncertainties, this may give an unacceptable uncertainty for the intended test system.

One possible alternative is to calibrate the response of the photodiode combined with the rf power sensor. This method totally eliminates uncertainties due to power sensor calibration and impedance mismatch. When the photodiode/power sensor combination transfer standard is used in the ratio test system, the combined frequency response is used to find the modulation depth of the source

$$M_O^2 = \left[\frac{1}{\mathbb{R}^2(f)} \right] \frac{P_{m:ref}}{0.5 \langle i_{dc:ref}^2 \rangle R_L} . \quad (\text{A8})$$

The normalized response of the DUT is then found using eq (A5), the dc photocurrent, and the rf power (including all calibration factors) from the DUT

$$\mathfrak{R}_{DUT}^2(f) = \left[\frac{1}{M_O^2} \right] \frac{P_{rf:DUT}}{0.5 \langle i_{dc:DUT}^2 \rangle R_L} . \quad (\text{A9})$$

In some test applications it may be preferable to measure the DUT's frequency response in terms of the coupling ratio instead of the bias current or average power. This may be the case when the DUT has poor dc stability or when the frequency response will be normalized to the response at a specific frequency (eliminating the coupling ratio). In this case eqs (A8) and (A9) can be combined to give

$$\mathfrak{R}_{DUT}^2(f) = \frac{P_{rf:DUT}}{P_{m:ref}} \mathbb{R}^2(f) \beta^2, \quad (\text{A10})$$

where β is the ratio of the optical power coupled to the reference arm to the power coupled to the test arm.

In the case of the amplified receiver described in Appendix D the combined response of the DUT is

$$\begin{aligned} g^2(f) &= \frac{G^2(f)}{C} \\ &= \frac{2R_L P_m}{P_{avg}^2} \end{aligned} \quad (\text{A11})$$

and can be used to find the modulation depth of the source from the equation

$$M_O^2 = \frac{2R_L P_{m:ref}}{g^2(f) P_{avg:ref}^2} . \quad (\text{A12})$$

The DUT's response is then

$$G_{DUT}^2(f) = \frac{2R_L P_{rf,DUT}}{M_O^2 P_{avg,DUT}^2} \quad (A13)$$

A.3 Sources of uncertainty in ratio measurement system

The following is a brief list of error sources that must be considered when designing a ratio test system.

Type of photoreceiver specimen: Equations (A9), (A10), and (A13) include the rf power measured from the DUT. If the DUT is a photoreceiver, the power must be measured with some kind of electrical transducer that will indicate how much electrical power is being generated. The calibration factor and impedance mismatch of this transducer must also be included in the customer's error budget. However, if the DUT is a device such as a lightwave communications analyzer or lightwave spectrum analyzer, which includes the transducer, the frequency response of the device as a whole is measured, eliminating calibration factor and mismatch uncertainties.

Spurious harmonics: Nonlinearities in directly modulated lasers, over driving, or inaccurate bias of external modulators can cause some harmonic content [A1]. The rf signal generator can also be a source of spurious harmonic and nonharmonic signals. Since the rf power sensor is not frequency selective, energy at spurious frequencies gives a systematic error. Assuming that the power sensor acts as a true rms detector, the powers add arithmetically. To keep the increase in uncertainty below 10 %, the total harmonic power must be more than 22 dB lower than the fundamental.

Relative intensity noise: Again, energy at frequencies other than the modulation frequency can give systematic errors.

Wavelength dependence: Wavelength dependence of a photodiode is a complicated function of the depletion region thickness, intrinsic layer thickness, bias voltage, and other parameters. The variation in response due to wavelength can be as much as several tenths of a decibel [A1]. Etalon effects inside the detector can cause relatively large changes in the dc responsivity in a way which is not directly measured if the bias current is not monitored. This effect can be minimized by operating the ratio test system at the same wavelength as the original calibration or corrections can be performed if the transfer standard can be accurately modeled.

Reference

A1. Hale, P. D.; Humphreys, D. A.; Gifford, A. D. Photodetector frequency response measurements at NIST, US, and NPL, UK: preliminary results of a standards laboratory comparison. *Proc. SPIE*, vol. 2149, pp. 345-355; 1994.

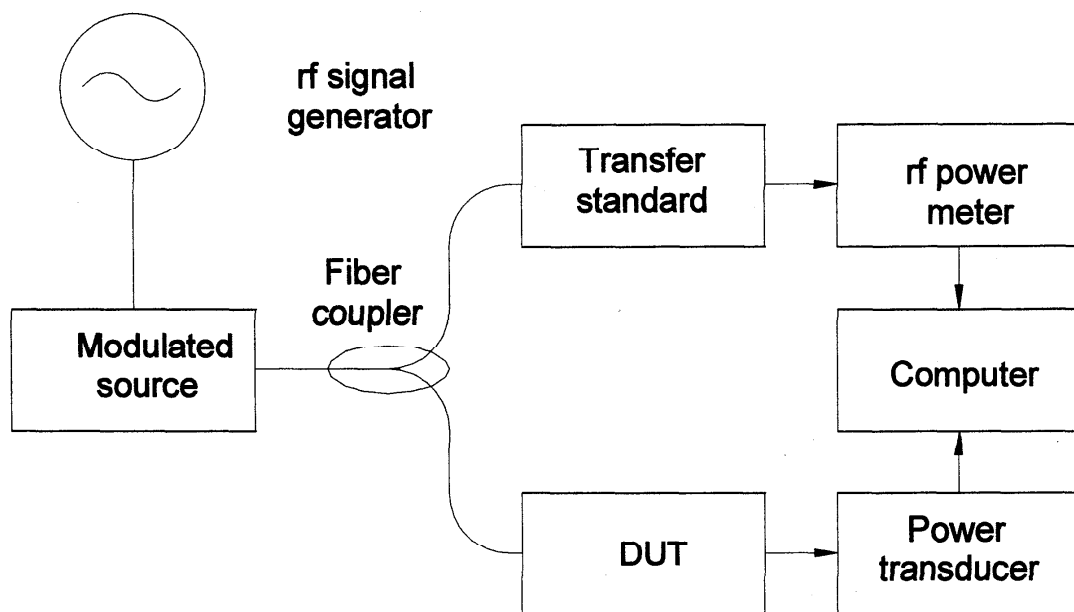


Figure A1. Ratio measurement system.

Appendix B: Heterodyne system with unequal powers

The powers from each laser incident on the detector may not be equal. In this case it is possible to formulate the expression for the normalized response in a way that eliminates error from the assumption that the powers are equal used in eq (6). But first it is illustrative to calculate the error induced by small deviations from equality. Let the optical powers be nearly equal, so that $P_{O1} = P_O$ and $P_{O2} = P_O + \delta$, where $\delta \ll P_O$. Then

$$(P_{O1} + P_{O2})^2 = 4(P_O^2 + P_O\delta) + \delta^2, \quad (\text{B1})$$

$$\begin{aligned} 2(P_{O1}P_{O2}) &= 2(P_O^2 + P_O\delta) \\ &\approx \frac{1}{2}(P_{O1} + P_{O2})^2. \end{aligned} \quad (\text{B2})$$

The last two lines of eq (6) then follow from eqs (B1) and (B2). The error caused by a small perturbation can then be approximated as

$$\begin{aligned} \frac{2P_{rf}}{\langle i_{dc}^2 \rangle R_L} &= \frac{\langle i_{rf}^2 \rangle R_L}{0.5 \langle i_{DC}^2 \rangle R_L} \\ &= \frac{2(P_{O1}P_{O2})R^2(f)}{0.5(P_{O1} + P_{O2})^2 R^2(0)} \\ &= \frac{2(P_O + \delta)P_O}{0.5(2P_O + \delta)^2} \mathfrak{R}^2(f) \\ &= \mathfrak{R}^2(f) \frac{\left(1 + \frac{\delta}{P_O}\right)}{\left(1 + \frac{\delta}{2P_O}\right)^2} \\ &\approx \mathfrak{R}^2(f) \left(1 - \frac{1}{4} \left(\frac{\delta}{P_O}\right)^2 + \dots\right). \end{aligned} \quad (\text{B3})$$

Hence, a 4 % fluctuation in P_{O2} will cause a 0.04 % or 0.0017 dB change in the measured value of $\mathfrak{R}^2(f)$.

On the other hand, large differences between the laser powers can lead to large errors in eq (6), even if the individual photocurrents are known. This error is shown in figure B1. This problem can be overcome by monitoring the individual photocurrents and using the exact ratio

$$\mathfrak{R}^2(f) \equiv \frac{P_{rf}}{2i_1 i_2 R_L} \quad (\text{B4})$$

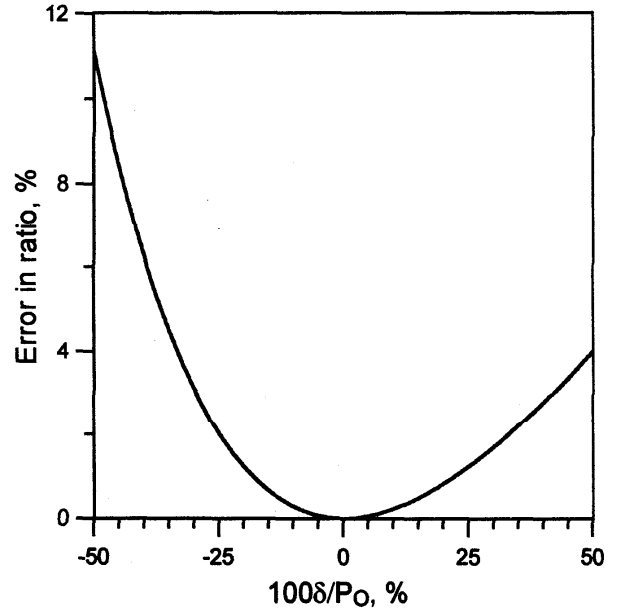


Figure B1. Error in ratio if total current is used instead of product of individual currents in eq (6).

Appendix C: The meaning of normalized response and 0 dB

A simple interpretation of the normalized response is the ratio of the rf responsivity (referred to the output (rf) port) to the dc responsivity (referred to the bias (dc) port). A normalized response of 0 dB then can be interpreted as the dc and rf responsivities (as defined in eq (4)) being equal. Since the rf responsivity is referred to the output port, the effect of any attenuators in the output path will be shown as an offset. For example, a detector followed by a 6 dB matching pad will show a normalized response that approaches -6 dB at low frequencies.

Another interpretation for 0 dB is that the rf signal from the photodiode is the maximum possible without driving it into forward conduction. That is, if the dc current is i_0 then the rf current has a maximum of $+2i_0$ and a minimum of 0.

The normalized response may be greater than 0 dB in steady state operation when the detector has some gain or the detector includes some inductive resonance. In the latter case, the diode current source drives an LRC tank circuit.

Appendix D: Photoreceiver with no access to bias monitor

D.1 Expression of absolute responsivity in terms of measured quantities

Some optical receivers will not allow access to the dc photocurrent or bias current. In this case it is necessary to measure the rf power generated relative to the optical power incident on the receiver. Since most high speed receivers are fiber-pigtailed and connectorized, it is difficult to measure the exact optical power that is incident on the receiver because of poor connector repeatability. This Appendix considers this situation. At this time, measurement of a receiver that does not have access to the bias current is offered only as a Special Test. It is desirable in some applications to know the absolute voltage response of the photoreceiver. An amplified photoreceiver commonly requires this type of characterization. This Appendix will demonstrate the formalism used in calculating voltage response.

For a photoreceiver without a bias current monitor, the system in figure 1 includes a 10 dB (nominal) optical coupler that monitors the total power from the lasers during a frequency scan. The power incident on the DUT is inferred from the coupler monitor port. The voltage that the receiver delivers to a load R_L is given by

$$V_p(f, t) = (P_{O1} + P_{O2})G(0) + 2\sqrt{P_{O1}P_{O2}}G(f)\cos(2\pi ft), \quad (D1)$$

where $G(f)$ is the amplified response of the detector (in V/W) at frequency f . The first term on the right side is the average dc signal, and the second term is the rf signal. The voltage response is found in a similar manner to eq (6) and is

$$G^2(f) = \frac{2R_L P_{rf}}{P_{avg}^2}, \quad (D2)$$

where $P_{avg} = P_{O1} + P_{O2}$ is the average (dc) optical power incident on the detector and P_{rf} is the electrical power delivered to a load R_L (the power sensor). This ratio is insensitive to small changes in power from either laser because the powers from the two lasers are nearly equal. If the voltage response is measured in dB (re 1 V/W), rf power in decibels (re: 1 mW), the average optical power is in decibels (re: 1 mW), and $R_L = 50 \Omega$, eq (6) can be written as [2]

$$20\log(G(f)) = 50 + \phi_{rf} - 2\phi_{avg}, \quad (D3)$$

where ϕ denotes a power measured in decibels (re: 1 mW).

D.2 Uncertainties of amplified receiver/power sensor combined response

Typical uncertainties for the receiver are listed in table D1. The dominant uncertainties are fiber connector insertion loss, power meter scaling, coupling ratio measurement, and power sensor

noise. Offset correction for the fiber connector insertion loss must be included to reduce the relative uncertainty to an acceptable level. The uncertainty in the absolute level still remains and can not be characterized within the tolerances that are typically required.

Coupling ratio: The coupling ratio is measured at the beginning of a measurement and then the 10 % port is monitored during the scan to infer the power reaching the receiver. The fiber-to-air launch from the coupler monitor port into the power meter is terminated with a connector angled at 8° to minimize coherent multiple path effects. Coherent effects due to nonzero return loss (typically 30 dB) give repeatable systematic uncertainties of about 0.35 % (1σ). Coupling ratio drift during the scan is random and is included in the repeatability described above. An additional error in monitoring the optical power is sometimes observed if there are etalon effects in the thin photodiode or between the fiber and detector. This causes the optical power measured by the monitor to be different from the actual power which is coupled into the photodiode and can be a significant error over a large bandwidth.

Receiver linearity: Since the power detection is not frequency selective, harmonics of the modulated signal due to nonlinearity give an error in the rf power measurement. To characterize the receiver nonlinearity the optical power can be varied and harmonics measured on an electrical spectrum analyzer. An optimum average optical power input is a compromise between receiver nonlinearity and power sensor noise.

Receiver stability: Measurements at frequencies well above the amplified receiver's cut off can show additional instability. This may be related to the low open loop gain of the receiver amplifier at these frequencies (see repeatability at 1500 MHz in table D1).

Receiver noise: Some broadband receivers generate noise power significantly higher than the power sensor noise floor, giving poor dynamic range in the heterodyne measurements. Often the noise power is stable and can be subtracted from the measured power in the heterodyne system, giving significant improvements in the measurement dynamic range.

Table D1. Summary of typical frequency response measurement uncertainties for the amplified photoreceiver (nominal bandwidth of 0.8 GHz) with thermal rf power sensor.

Source of uncertainty	Uncertainty, $k = 1, \%$
Type A	
Measurement repeatability @ 0.010 GHz	0.05
@ 1.5 GHz	1.1
Offset correction s_a	0.007
Environmental effects s_e (f in GHz)	$0.106 + 0.00064 f + 0.00024 f^2$
Type B	
Meter scaling	0.5
Meter offset	0.023
Coupling ratio	0.35
Optical power drift (power matching)	0.06
Receiver linearity, estimated from proto 900	0.1
Power sensor noise, @ 0.01 GHz	0.2
@ 1.5 GHz	3.8
Total uncertainty, @ 0.01 GHz	0.66
@ 1.5 GHz	4.0
Expanded uncertainty (coverage factor $k = 2$), @ 0.01 GHz	1.3 (0.06 dB)
@ 1.5 GHz	8.0 (0.34 dB)

Appendix E. Sample calibration certificate

U.S. DEPARTMENT OF COMMERCE
NATIONAL INSTITUTE OF STANDARDS AND TECHNOLOGY
ELECTRONICS AND ELECTRICAL ENGINEERING LABORATORY
Boulder, Colorado 80303

REPORT OF CALIBRATION

Reference Receiver

XXX photodiode, Serial No. xxxxxxxx
XXX power sensor, Serial No. xxxxxxxxxx
XXX 3 dB attenuator, Serial No. xxxxxx

Submitted by:
Manufacturer's Name
Street Address
City, State Zip

The combined normalized frequency response of the Reference Receiver was measured at 1.319 μm . The Reference Receiver consists of a photodiode with bias current monitor circuit, a 3 dB attenuator or bias tee, and an rf power sensor. Measurements were made in the following frequency bands:

1. 200 - 900 kHz, 100 kHz steps
2. 1 - 40 MHz, 0.5 MHz steps
3. 41 - 119 MHz, 1 MHz steps
4. 120 - 600 MHz, 3 MHz steps
5. 630 - 4200 MHz, 15 MHz steps
6. 4250 - 40000 MHz, 50 MHz steps
7. 40100 - 50000 MHz, 100 MHz steps

Since the power sensors are fixed they can not be referred to the 50 MHz reference oscillator on the power meter. Hence the "combined normalized response" $R^2(f)$ was further normalized to 1 (0 dB) at 50 MHz. Bands were spliced together with offset corrections typically on the order of 0.01 dB or less. The typical uncertainty in the measurement results is less than ± 0.05 dB (coverage factor $k = 2$) below 36 GHz and is dominated by uncertainties in the power meter.

Page: Page x of y
Calibration No.: xxxxx
Date of Report: month xx, 199x 40

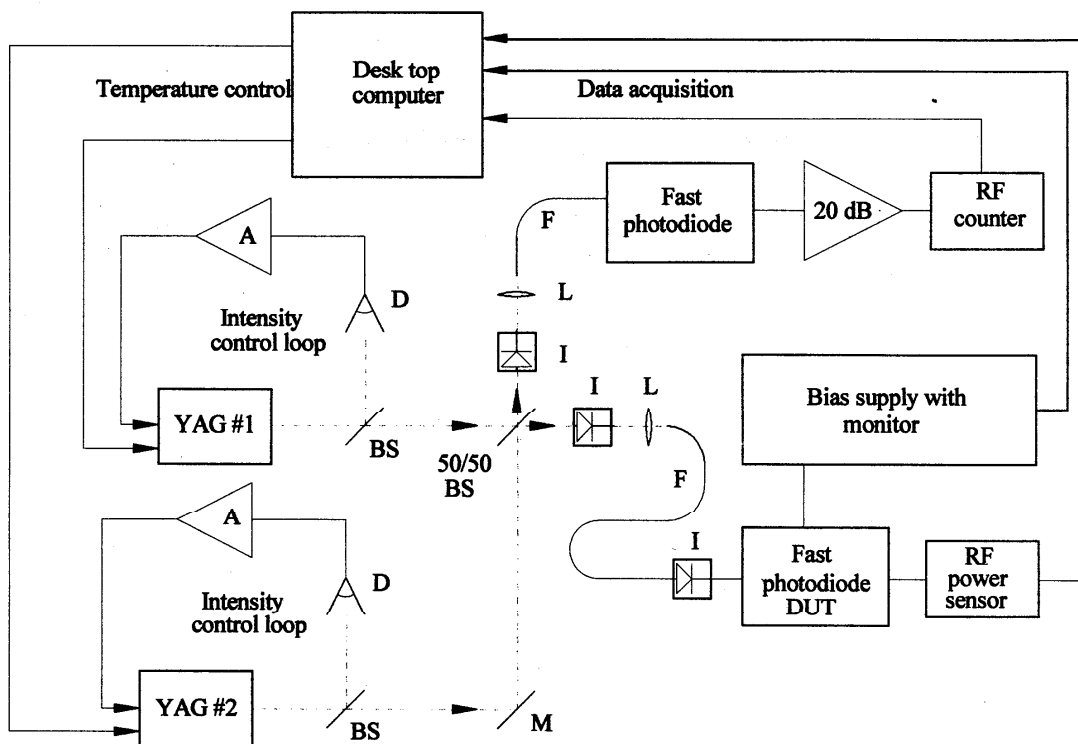


Figure 1. Simplified schematic of the NIST Nd:YAG heterodyne system. Labeled components are beamsplitter (BS), mirror (M), isolator (I), lens (L), fiber (F), large area detector (D), and integrating amplifier (A).

Above 40 GHz the noise of the power sensor becomes the dominant uncertainty.

Results for this Calibration are reported in a graph on page 8 of this report and on a 3.5 inch DOS compatible disk in ASCII format.

NIST Nd:YAG heterodyne measurement at 1.319 μm

NIST uses a Nd:YAG heterodyne system for measuring scalar frequency response because the excitation of the detector can be calculated from first principles. A schematic of the heterodyne system is shown in Figure 1. The system uses two single-mode monolithic-ring Nd:YAG lasers operating at 1.319 μm . The frequency of each laser can be tuned thermally to give beat frequencies between dc and 65 GHz; the beats have a bandwidth of the order of 10 kHz. The beat frequencies below 40 GHz are measured with an rf counter. Frequencies above 40 GHz are down converted to a frequency that the counter can measure by mixing with a Gunn oscillator operating at 62.14 ± 0.015 GHz. As the frequency is scanned, data are acquired automatically. The resolution of the system is limited by the scan rate, the frequency jitter, and the time constants

of the data acquisition equipment. At present, the highest resolution achievable in swept operation is about 300 kHz. Finer resolution (< 100 Hz) is attained using a phase-locked loop (not shown in figure 1) at frequencies between 300 kHz and 1 GHz. The lasers are intensity stabilized so that nearly equal power from each laser is delivered to the photodiode as measured by the bias current monitor. The combined laser beams pass through a polarizing isolator so that the signal from each laser is in the same polarization state when it reaches the photodiode ensuring nearly 100 % modulation depth. The total optical power incident on the photodiode is

$$P_{total}(t) = (P_{O1} + P_{O2}) + 2\sqrt{P_{O1}P_{O2}} \cos(2\pi ft) , \quad (1)$$

and the photocurrent generated is given by

$$i_p(f,t) = (P_{O1} + P_{O2})R(0) + 2\sqrt{P_{O1}P_{O2}}R(f)\cos(2\pi ft) , \quad (2)$$

where P_{O1} and P_{O2} are the optical powers delivered to the detector from the lasers and $R(f)$ is the responsivity of the detector (in A/W) at frequency f . The first term on the right side is the dc photocurrent, which flows through the bias supply, and the second term is the rf photocurrent which flows through the rf load through a high-pass filter. The mean-squared photocurrent generated by the photodiode is

$$\langle i_p^2 \rangle = (P_{O1} + P_{O2})^2 R^2(0) + 2P_{O1}P_{O2}R^2(f) \quad (3)$$

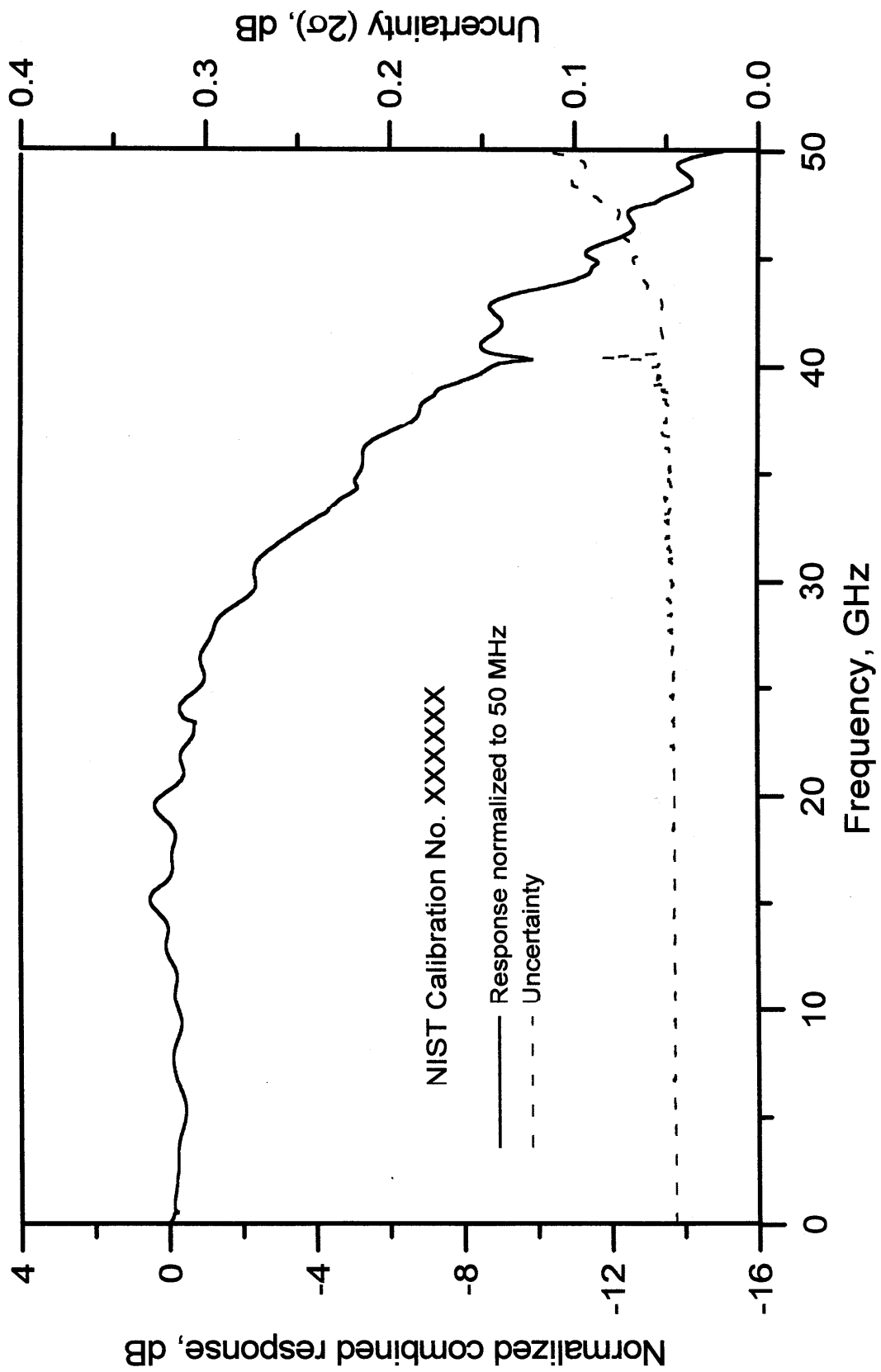
where the first term on the right side is a dc term and the second is an ac term; hence

$$\langle i_p^2 \rangle = \langle i_{dc}^2 \rangle + \langle i_{rf}^2 \rangle . \quad (4)$$

These terms are proportional to the electrical power generated by the photodiode. If P_{O1} is nearly equal to P_{O2} , then $2(P_{O1}P_{O2})$ is, to first order, equal to $0.5(P_{O1}+P_{O2})^2$. The normalized frequency response $\mathfrak{R}^2(f)$, which is defined as $R^2(f)/R^2(0)$, can then be found by taking the ratio of the rf electrical power P_{rf} to half the dc electrical power delivered to a load R_L ,

$$\begin{aligned} \frac{2P_{rf}}{\langle i_{dc}^2 \rangle R_L} &= \frac{\langle i_{rf}^2 \rangle R_L}{0.5 \langle i_{dc}^2 \rangle R_L} \\ &= \frac{2(P_{O1}P_{O2})R^2(f)R_L}{0.5(P_{O1} + P_{O2})^2 R^2(0)R_L} \\ &\approx \frac{R^2(f)}{R^2(0)} . \end{aligned} \quad (5)$$

P_{rf} is a function of frequency. It includes corrections for sensor calibration factor and electrical



Appendix F. Shipping instructions

Equipment should be shipped in well-padded foam, or otherwise mechanical-shock insulated cases, appropriate for reshipment back to the customer. Operation instructions or instruction manuals should be included, as well as the customer chosen set-up parameters for instrument functions, including bias voltage, bias current, frequency points required, which connections (if any) should be left unchanged, and any other special instructions. The customer should include all cables and connectors that are necessary to calibrate the equipment as specified. Depending on the power meter model and manufacturer, it may be necessary to include the power meter and instruction manual.

U.S. Department of Commerce
National Institute of Standards
and Technology
325 Broadway
Boulder, Colorado 80303-3328

Official Business
Penalty for Private Use \$300